Molecular Systems Biology 5; Article number 252; doi:10.1038/msb.2009.10
Citation: ***Molecular Systems Biology*** **5:252**

www.molecularsystemsbiology.com

molecular systems biology

A systems approach to prion disease

Daehee Hwang[1,2,8], Inyoul Y Lee[1,8], Hyuntae Yoo[1,8], Nils Gehlenborg[1,3], Ji-Hoon Cho[2], Brianne Petritis[1], David Baxter[1], Rose Pitstick[4], Rebecca Young[4], Doug Spicer[4], Nathan D Price[7], John G Hohmann[5], Stephen J DeArmond[6], George A Carlson[4,*] and Leroy E Hood[1,*]

[1] Institute for Systems Biology, Seattle, WA, USA, [2] I-Bio Program & Department of Chemical Engineering, POSTECH, Pohang, Republic of Korea, [3] Microarray Team, European Bioinformatics Institute, Wellcome Trust Genome Campus, Cambridge, UK, [4] McLaughlin Research Institute, Great Falls, MT, USA, [5] Allen Brain Institute, Seattle, WA, USA, [6] Department of Pathology, University of California, San Francisco, CA, USA and [7] Department of Chemical and Biomolecular Engineering & Institute for Genomic Biology, University of Illinois, Urbana, IL, USA
[8] These authors contributed equally to this work
* Corresponding authors. GA Carlson, McLaughlin Research Institute, 1520 23rd Street South, Great Falls, MT 59405, USA. Tel.: +1 406 454 6044; Fax: +1 406 454 6019; E-mail: gac@po.mri.montana.edu or LE Hood, Institute for Systems Biology, 1441 North 34th Street, Seattle, WA 98103, USA. Tel.: +1 206 732 1201; Fax: +1 206 732 1254; E-mail: lhood@systemsbiology.org

Received 27.11.08; accepted 20.1.09

Prions cause transmissible neurodegenerative diseases and replicate by conformational conversion of normal benign forms of prion protein (PrP^C) to disease-causing PrP^{Sc} isoforms. A systems approach to disease postulates that disease arises from perturbation of biological networks in the relevant organ. We tracked global gene expression in the brains of eight distinct mouse strain–prion strain combinations throughout the progression of the disease to capture the effects of prion strain, host genetics, and PrP concentration on disease incubation time. Subtractive analyses exploiting various aspects of prion biology and infection identified a core of 333 differentially expressed genes (DEGs) that appeared central to prion disease. DEGs were mapped into functional pathways and networks reflecting defined neuropathological events and PrP^{Sc} replication and accumulation, enabling the identification of novel modules and modules that may be involved in genetic effects on incubation time and in prion strain specificity. Our systems analysis provides a comprehensive basis for developing models for prion replication and disease, and suggests some possible therapeutic approaches.
Molecular Systems Biology 24 March 2009; doi:10.1038/msb.2009.10
Subject Categories: neuroscience; molecular biology of disease
Keywords: microarray; network analysis; neurodegenerative disease; prion

Introduction

Systems approaches to disease arise from a simple hypothesis—disease emerges from the functioning of one or more disease-perturbed networks (genetic and/or environmental perturbations) that alter the levels of proteins and other informational molecules controlled by these networks. The dynamically changing levels of disease-perturbed proteins (networks) across disease progression presumably explain the mechanisms of the disease. Systems approaches to biology or medicine have two cardinal features: (1) global analyses to generate comprehensive data sets in the disease-relevant organ or cells across the dynamically changing disease process (e.g. all mRNA, miRNA, or protein levels) and (2) the integration of different levels of biological information (DNA, mRNA, miRNA, protein, interactions, metabolites, networks, tissues, organs, and phenotypes) to generate hypotheses about the fundamental principles of the disease (Hood *et al*, 2004). In this study, we present a systems biology approach that effectively uses these two features, uses multiple inbred mouse strains, uses a deep understanding of prion biology and applies statistical data integration methods to deal with two striking challenges: (1) sorting out the signal-to-noise issues arising from the global disease-associated changes as both measurement noise and biological noise and (2) reducing enormous data dimensionality so that the processes can be identified and visualized for study. The keys to reducing this noise are to apply a deep understanding of biology to carry out subtractive data analyses that focus on particular biological issues—as well as to use integrative statistical methods. We applied the systems approach to experimentally tractable neurodegenerative diseases caused by prion infection of mice. Analysis of a large data set (~20 million data points) revealed slightly more than 300 differentially expressed genes (DEGs) that may encode fundamental processes in prion disease.

Prions are unique among transmissible, disease-causing agents in that they replicate by conformational conversion of normal benign forms of prion protein (PrP^C) to disease-specific

PrP^{Sc} isoforms. Neuropathological features common to all prion diseases in mammals, which include bovine spongiform encephalopathy (BSE) in cows, Creutzfeldt–Jakob disease (CJD) in humans, and scrapie in sheep, can be conveniently subdivided into four processes: prion (PrP^{Sc}) replication and accumulation (Prusiner, 2003), synaptic degeneration (Ishikura *et al*, 2005), microglia and astrocyte activation (Rezaie and Lantos, 2001; Perry *et al*, 2002), and neuronal cell death (Liberski *et al*, 2004). There exist distinct strains of infectious prions that have different properties (e.g. duration of incubation time, sites of infection in the brain, and so on) that presumably arise from distinct structural forms of misfolded prion proteins (e.g. distinct three-dimensional structures and/or chemical modifications).

Changes in gene expression induced by prion infection were followed at multiple time points in diverse mouse–prion combinations over the entire course of the incubation times with end points ranging from 56 to 392 days (Figure 1 and Table I: incubation time is defined as the time period from prion infection to an end point, where all mice in each combination showed end-stage clinical signs of prion disease (except for *Prnp*-null (0/0) mice)). Three factors responsible for this wide range in incubation times are represented in our mouse strain–prion strain combinations: (1) distinct prion strains can produce different incubation times in genetically identical hosts, (2) host genotype determines incubation times for a prion strain with the allelic forms of the PrP gene (*Prnp*) having the strongest effect, and (3) concentrations of PrP affect the incubation times. Infected animals exhibit no signs of illness over most of their incubation periods. The dynamically changing DEGs were mapped onto a series of known protein interaction maps and integrated with histopathological data on PrP^{Sc} accumulation and distribution in the brain at multiple time points during disease incubation. This integration was used to develop hypothetical molecular subnetworks presumably encoding various cellular processes that are perturbed by prion infection and these hypotheses were validated by statistical and biological assessments of the DEGs central to prion disease. The networks identify perturbations of cellular processes that appear essential for prion replication and also the interactions of such processes with subnetworks involved in pathological changes. With the exception of the prion replication and accumulation network, similar changing network processes are seen in other neurodegenerative disorders, including Alzheimer's disease (Bossy-Wetzel *et al*, 2004; Spires and Hannan, 2007).

It is important to stress that dynamic biological networks may change in two ways—the transcripts of the nodal points in the network may change in concentration or chemical structure; the architecture of the network may change in the nature of its connections or interactions. One of the grand challenges of systems biology is to develop methods that may easily measure the dynamically changing architecture of networks—and currently we are unfortunately forced to map or correlate the dynamical changes in transcripts, histopathology and clinical signs onto networks, the dynamics of which are revealed only by changes in the concentrations of mRNAs. Even with this coarse granularity of understanding, powerful insights into the nature of prion disease emerge from the correlation of histopathology, clinical signs and dynamical networks—explaining much of what we already know about this disease mechanistically in terms of biological network behavior as well as beginning to providing insights into new pathogenic mechanisms and potential strategies for therapeutic intervention.

Results

Microarray analysis of gene expression

To facilitate the identification of differential gene expression relevant to essential processes in prion replication and disease,

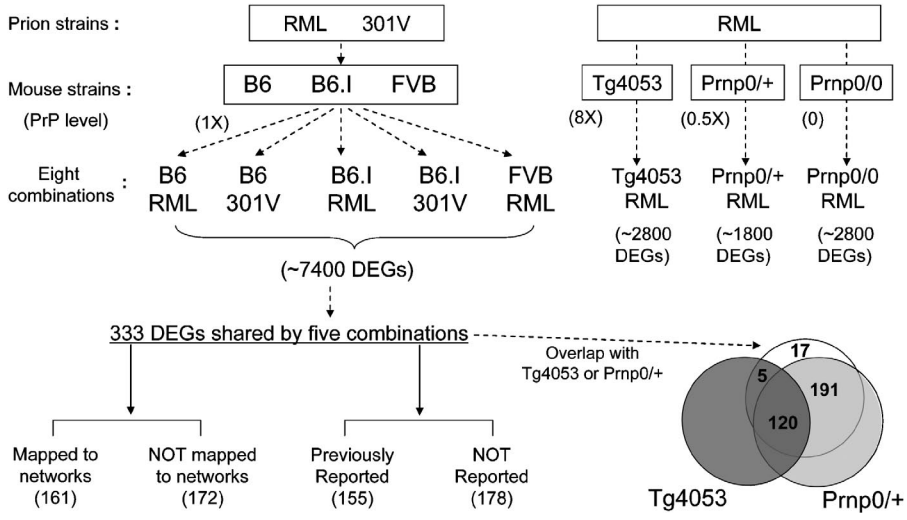

Figure 1 Strategies for identification of 333 core differentially expressed genes (DEGs) and their functional analysis in mouse prion diseases. Two prion strains (RML and 301V) were used for inoculating mice from six different genetic backgrounds (B6, B6.I, FVB, Tg4053, 0/+, and 0/0) to generate eight prion–mouse combinations. From the list of 7400 DEGs identified from at least one of the five combinations with normal levels of prion protein (1X), 333 DEGs shared by all five were selected through novel statistical methods to represent perturbed networks essential to prion pathophysiology. Venn diagram shows the overlap of the 333 DEGs with DEGs from Tg4053-RML (mice expressing eight times of normal prion protein levels) and from 0/+-RML (mice expressing one-half of normal prion protein levels). Among 333 DEGs, 161 genes were mapped to networks through protein–protein interaction network or metabolic pathways. Also, by comparison of 333 DEGs with previous prion microarray studies, we identified 178 DEGs that have not been reported in connection with prion disease.

Table I Mouse strain–prion strain combinations

Mouse strain	*Prnp* genotype	Prion strain	End point[a] (days/weeks)	Harvest interval[b] (weeks)
C57BL/6J (B6)	*a/a*	RML	161/23	2
C57BL/6J (B6)	*a/a*	301V	287/41	4
C57BL/6.I-1 (B6.I)	*b/b*	RML	336/48	4
C57BL/6.I-1 (B6.I)	*b/b*	301V	126/18	2
FVB/NCr (FVB)	*a/a*	RML	154/22	2
FVB-Tg(PrP-A)4053 (Tg4053)	*>30a*	RML	56/8	1
(FVB x FVB.129-*Prnp*^{tm1Zrch})F1 (0/+)	*a/0*	RML	392/56	4
FVB.129-*Prnp*^{tm1Zrch} (0/0)	*0/0*	RML	196/28[c]	4

[a]End point is equivalent to the incubation time in this study, which is defined as the interval between prion inoculation to end point. With the exception of 0/0 mice, all animals were at the terminal stages of disease when killed for brain harvest. For each combination, a set of mice was inoculated with brain homogenate from normal mice and brains were harvested at the same time points as prion-infected mice.
[b]Brains from three mice were taken at each time point. In a few instances, the interval deviated from that shown. For example, the final interval for B6-RML was 1 week due to severity of illness in these mice. The actual intervals are indicated in figures that follow.
[c]Additional three RML-inoculated and three normal brain homogenate-inoculated 0/0 mice were aged 357 days (51 weeks).

we selected the mouse strain–prion strain combinations shown in Table I. The combinations reflect three different factors that can dramatically impact the incubation time: prion strain, host genotype, and PrP concentration. Two prion strains, Rocky Mountain Lab (RML) mouse-adapted scrapie prions and 301V mouse-adapted BSE prions, produce dramatically different incubation times in a single inbred strain of mice. For example, C57BL/6J (B6) mice inoculated with RML (B6-RML) have short incubation times compared with B6 mice inoculated with 301V prions (B6-301V) (see Table I). Host genotype also affects incubation time (Westaway *et al*, 1987). Indeed, alternative alleles of the PrP gene, *Prnp*, encode distinct proteins that dramatically alter incubation time. B6 and B6.I-*Prnp*^{b} (B6.I) mice are congenic for the interval on Chr 2 that contains *Prnp* (Carlson *et al*, 1993, 1994). B6 mice inoculated with RML prions (B6-RML) have short incubation times, whereas B6.I (*Prnp*^{b}) mice inoculated with the same prion strain (B6.I-RML) have long RML incubation times owing to their different PrP sequences (Westaway *et al*, 1987). The converse is true for 301V prions (B6-301V and B6.I-301V) with B6.I mice having shorter incubation times than B6 mice (Bruce *et al*, 1994; Carlson *et al*, 1994). Thus, it is important to stress that long incubation time is not an inherent property of either *Prnp* genotype or prion strain, but reflects interactions between the host and the agent.

PrP concentration also affects incubation time. The FVB/NCr (FVB) genetic background was used for testing effects of the level of PrP expression on gene expression in prion disease. Mice that are heterozygous for a null allele of *Prnp*, (FVB.129-*Prnp*^{tm1Zrch} × FVB)F1 (0/+), express half the amount of PrP as FVB, and have very long incubation times in spite of accumulating high levels of PrP^{Sc} in a long preclinical stage (Bueler *et al*, 1994; Manson *et al*, 1994). On the other hand, FVB-Tg(PrP-A)4053 mice (Tg4053) that overexpress PrP transgenes have very short incubation times (Carlson *et al*, 1994). FVB, 0/+, and Tg4053 mice were inoculated with RML prions (FVB-RML, 0/+-RML, and Tg4053-RML). FVB.129-*Prnp*^{tm1Zrch} mice (0/0) that lack PrP entirely, cannot be infected with prions (Bueler *et al*, 1993) and do not develop disease, were also inoculated with RML prions to eliminate DEGs induced by prions that are not relevant to prion disease. Only one statistically significant DEG (*Itgam*) was found in 0/0 mice—reassuring us that the statistics and subtractive analyses of dynamically changing transcriptomes guided by prion biology worked effectively.

Thus, the eight mouse strain–prion strain combinations can be assigned to different groups to emphasize different aspects of disease and the DEGs generated by these groups can be used in subtractive comparisons to analyze discrete aspects of prion disease. Grouping B6-RML, B6-301V, B6.I-RML, B6.I-301V, and FVB-RML will emphasize DEGs induced by both prion strains and across incubation times; such shared DEGs are likely to reflect functionally important processes. The combinations also can be grouped according to prion strain for the identification of DEGs enriched in response to one strain versus the other (comparing B6-RML, B6.I-RML, and FVB-RML with B6-301V and B6.I-301V). Short incubation time combinations reflecting prion strain–PrP genotype interactions (B6-RML, B6.I-301V, and FVB-RML) also can be compared with long incubation time combinations (B6-301V and B6.I-RML). The genetically modified combinations (0/+-RML and Tg4053-RML) were used as biological filters whose incubation time differences reflected PrP concentration rather than PrP genotype.

Comparison of B6 and FVB mice inoculated with RML (B6-RML and FVB-RML) that do not have a large difference in prion incubation times served to filter out DEGs that presumably reflect mouse strain genetic polymorphisms (see Supplementary Figure S1 showing *Ccl12*, *Usp18*, and *Bst2* as examples of genes, the expression of which increased only in B6 mice).

Brains from three mice per group were harvested every 1, 2, or 4 weeks depending on the length of the incubation times as indicated in Table I (the idea was to have 8–10 sample comparisons across the incubation period). Comprehensive time course transcriptomic data sets were generated from each of the eight mouse strain–prion strain combinations using Affymetrix mouse array 430 2.0 chips (450 arrays, see Materials and methods and Supplementary information).

The noise in this enormous amount of data includes both (1) biological noise due to environment-induced or stochastic variation among replicate, genetically identical individual mice that could obscure meaningful, but small, differences coming from different prion strains, alternative alleles of *Prnp*, differences in PrP concentration, and the resulting differences in incubation time and dynamics of pathological changes and (2) technological noise from variation in prion inoculation

precision into the thalamus, sample preparation for array analysis, the array measurements themselves, and other factors. The majority of transcripts do not change their expression patterns as a result of prion disease, though some could be associated with prion disease despite no expression change—*Prnp* is the best-known example. The transcripts that are differentially expressed can also show different temporal patterns dependent on the mouse strain–prion strain combinations. The challenge here is to reliably detect initially small changes superimposed on a large more constant background. We developed an effective data analysis framework that can extract core prion-related signatures from such noise-corrupted data by resolving the noise-related problems. To cancel out responses caused by intracerebral inoculation and aging of the mice, we performed microarray analysis of age- and genotype-matched control mice inoculated with brain homogenates from normal mice at each time point; differential mRNA expression at each time point in each mouse–prion combination reflected subtraction of expression from the corresponding control mice. This minimized both biological and technological noises.

We developed a statistical method that effectively identified a core gene set, the expression levels of which were changed similarly across multiple mouse–prion combinations. The identification of this core gene set reduced the whole genome-scale data down to a smaller data set with potential prion disease association. Our method to identify shared expression patterns by integrating multiple mouse strain–prion strain data allowed the detection of differential signals that were marginal in some individual combinations but significant when considering all combinations together. Although analysis of DEGs using mRNA prepared from whole brain dilutes expression signals from individual brain regions, this integration-based gene selection compensates by its biological focus on changes that are relevant to the progression of pathology and prion replication. That is, this method can reliably select as DEGs the genes with marginal *P*-values (close to the cutoff) due to small expression changes (e.g. fold change=1.5) over time in the individual mouse–prion combinations by producing significant overall *P*-values ($<10^{-3}$) when the individual marginal *P*-values in multiple mouse–prion combinations were combined (details of the method described below). Using this method, we found that the overall *P*-values for such transcripts tend to be smaller than those of the transcripts that showed inconsistent temporal expression patterns (e.g. changed in some combinations and not changed in the others or changed in opposite directions) across the multiple mouse–prion combinations.

Shared DEGs in prion disease

To identify genes involved in essential processes related to prion pathogenesis, we first focused on the five prion strain-mouse strain combinations (B6-RML, B6.I-301V, B6-301V, B6.I-RML, and FVB-RML) that reflect *Prnp* allele- and prion strain-dependent short and long incubation times with normal levels of prion protein (Figure 1). We developed a novel statistical method (see Materials and methods and Supplementary information for further details) to identify the genes that are differentially expressed and also whose differential expression patterns are shared in the five combinations. We identified 333 DEGs (representing 428 probe sets, overall $P<10^{-3}$; see Supplementary Table S1 for the complete list) with shared temporal patterns of differential expression in the five core mouse–prion combinations. As will be presented later, these shared DEGs were also evaluated in 0/+ and Tg4053 mice where long and short incubation times are dependent on PrP concentration rather than on prion strain–PrP allotype interactions. Profiles for the top 20 shared DEGs with the lowest *P*-values (highest statistical significance for dynamic changes in prion disease) and for the bottom 20 DEGs at or near $P=10^{-3}$ (lowest statistical significance) are shown in Figures 2A and B. These profiles illustrate the range and patterns of shared expression across the five mouse–prion combinations used to identify shared transcripts as well as in 0/+ and Tg4053 mice inoculated with RML. The 333 shared DEGs did not change their levels in RML-inoculated 0/0 mice—supporting the contention from other subtractive analyses that these are reflections of the prion disease process.

Many of the highly significant DEGs had been identified in previous transcriptomic studies on differential gene expression in prion-diseased mice (Booth *et al*, 2004; Riemer *et al*, 2004; Xiang *et al*, 2004, 2007; Brown *et al*, 2005; Skinner *et al*, 2006; Sorensen *et al*, 2008). For example, of the top 20 DEGs in our study all but two (*Ifit1* and 0610011I04Rik) had been identified previously in at least one mouse strain–prion strain combination in one or more microarray studies. In contrast, only 9 of the bottom 20 genes of the core 333 gene list were found in previous studies (Figure 2B). Asterisks on the gene labels in Figures 2A and B indicate DEGs unique to this study. Overall, about half—178 of the 333 genes that we classified as shared—had not been identified previously as differentially expressed in prion-infected mice; only 11 of these were downregulated (Supplementary Table S1). Microarray data were validated using RT–PCR for 59 of the 333 shared genes as shown in Supplementary Figure S2. These shared DEGs were used as the basis for construction of hypothetical dynamic protein interaction networks for integration with pathological changes and PrP^{Sc} accumulation throughout the incubation period.

Integration of data from genetically modified mice to assess functional significance of DEGs

We examined the effects of PrP concentration on differential expression patterns in prion infection. These data can be useful, for example, in discriminating DEGs that may be involved in prion replication from those responsible for neuron dysfunction and death, and in distinguishing non-pathogenic responses to PrP^{Sc} accumulation from those likely to be responsible for clinical disease. Mice heterozygous for the null allele of *Prnp* (0/+) have very long incubation times. Although the rate of accumulation of PrP^{Sc} is slower than that in wild-type mice, proteinase K-resistant PrP^{Sc} eventually reaches levels that are very similar to those in terminal FVB mice well before any signs of disease occur (Figure 3A) (Bueler *et al*, 1994; Manson *et al*, 1994). Even 40 weeks after infection no clinical signs are apparent in 0/+ mice even though the level of accumulation and distribution of PrP^{Sc} is comparable to that in FVB mice exhibiting significant clinical signs

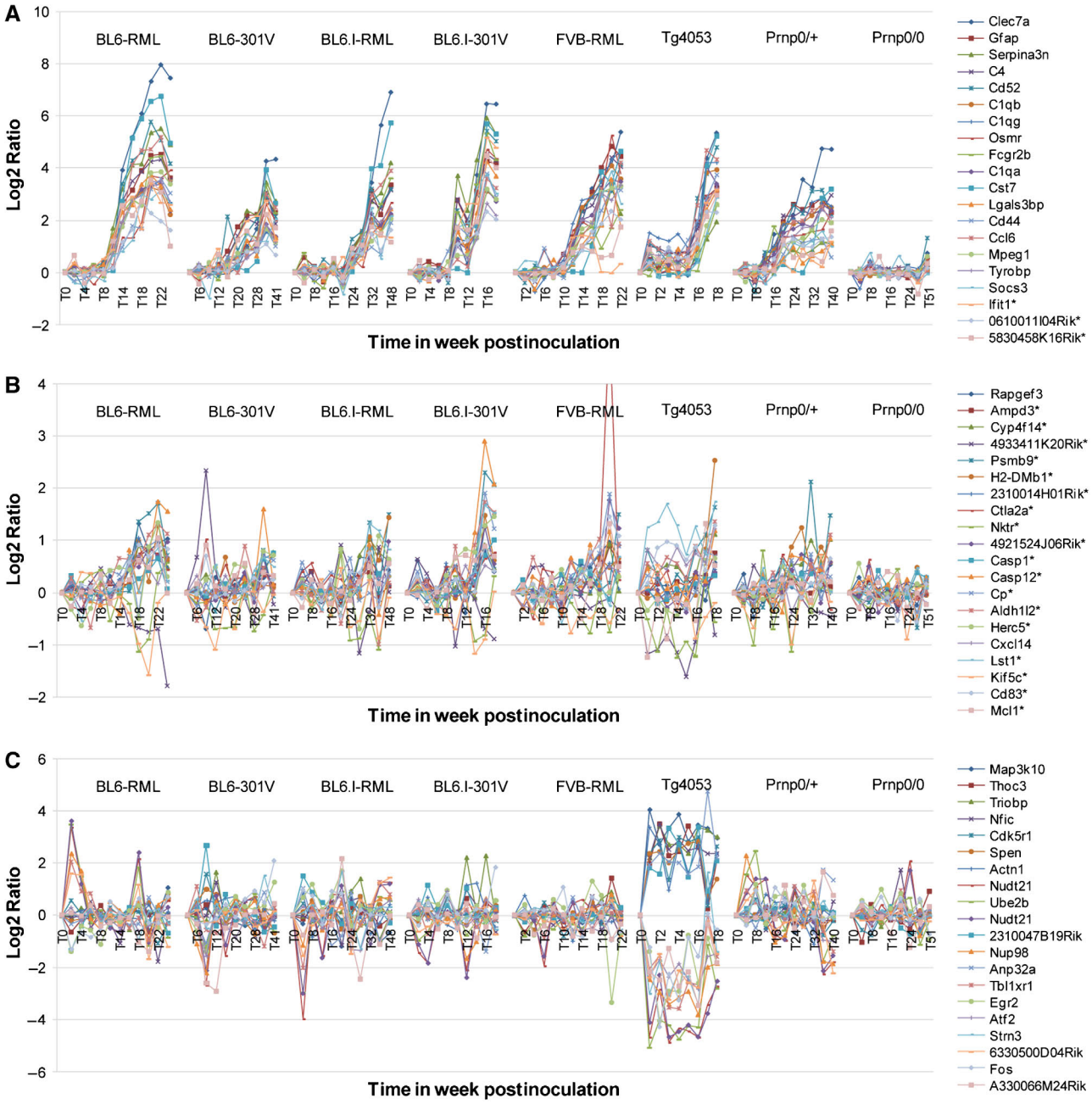

Figure 2 Expression profiles of genes shared among comparison of five mouse–prion combinations or unique to Tg4053-RML. Dynamic gene expression profiles in all eight mouse strain–prion strain combinations are shown for three cases in the order of B6-RML, B6-301V, B6.I-RML, B6.I-301V, FVB-RML, Tg4053-RML, 0/+-RML, and 0/0-RML: (**A**) top 20 genes with highest statistical significance for involvement in prion pathology among 333 differentially expressed genes (DEGs) shared by five combinations, B6-RML, B6-301V, B6.I-RML, B6.I-301V, and FVB-RML; (**B**) bottom 20 genes with lowest statistical significance for involvement in prion pathology among 333 shared DEGs; and (**C**) top 20 DEGs with highest statistical significance for involvement in prion pathology among RML-infected Tg4053 mice.

(Figure 3A). This suggests that early-appearing DEGs in 0/+ mice might be more relevant to prion replication and less pathogenic host responses to PrP^{Sc} accumulation than to neurodegeneration and cell death. The dramatic increase in scrapie survival times of 0/+ mice in spite of carrying similar amounts of PrP^{Sc} as seen in terminal wild-type FVB mice for more than 200 days is an apparent consequence of the lower steady-state level of PrP^{C} in the brains of 0/+ mice—about one-half of that in wild-type mice. Consequently, the rate of accumulation of PrP^{Sc} in the brain is significantly less than in wild-type mice as is the rate of accumulation of neurological damage that ultimately results in clinical signs (see histoblots in Figure 3A and in the Prion Disease DataBase (PDDB) website, http://prion.systemsbiology.net).

Among 333 shared DEGs gleaned from five prion–wild-type mouse strain combinations, 311 DEGs were changed in 0/+ mice ($P<0.05$; Supplementary information). A subset of the 311 DEGs shared by 0/+ were involved in key biological processes, as identified by analysis of their Gene Ontology (GO) annotations. These processes include complement activation,

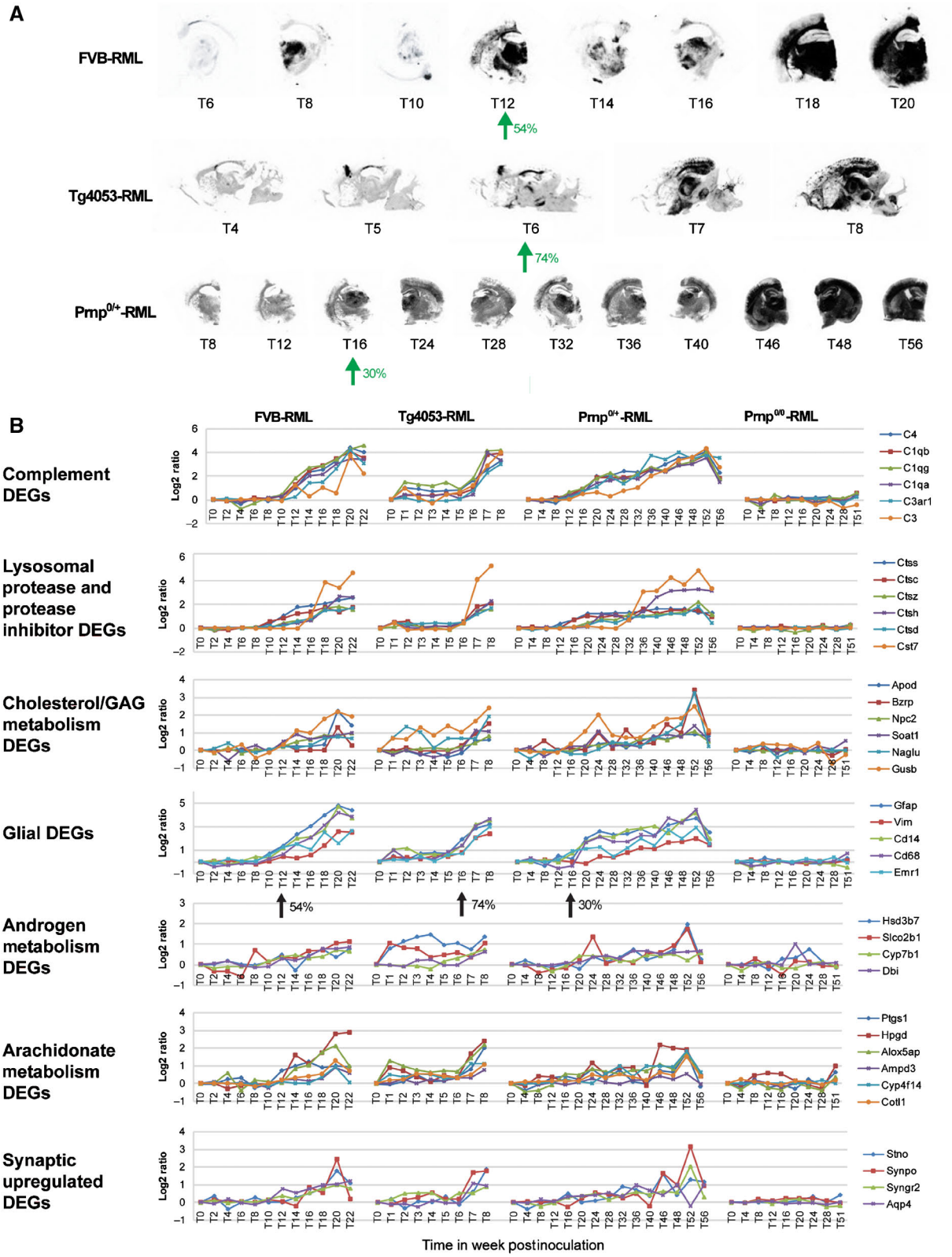

Figure 3 Time course histoblots and profiles of selected DEGs in three mouse strains with varying PrP^C concentration. (**A**) Histoblots are shown for dynamic patterns of accumulation of proteinase K-resistant PrP^{Sc} in brains of RML-infected mice with wild-type PrP^C concentration (FVB), half of wild-type PrP^C concentration (0/+), and approximately eight times of wild-type PrP^C concentration (Tg4053). (**B**) Expression profiles of shared DEGs representing key network modules are shown for FVB, Tg4053, and 0/+ mice. No significant changes were detected for these genes in mice lacking the Prnp gene (0/0). Percentage of the incubation times (incubation time is defined in this paper as the time period from prion inoculation to end point) for the time points when gene expression changes start to occur are indicated with arrows in histoblot series (A) and gene expression profiles (B).

lysosomal proteases, cholesterol synthesis/efflux, glycosaminoglycan (GAG) metabolism, and sphingolipid synthesis/degradation (Figure 3B). These results are consistent with these genes and their associated processes playing important roles in PrP^{Sc} replication and accumulation.

A significant question in prion disease is whether glial (both microglia and astrocytes) activation is triggered by accumulation of PrP^{Sc} directly or by neurodegenerative changes in neurons due to prion replication. The results in Figure 3B show that genes associated with microglial proliferation and astrocytosis (*Cd14*, *Cd68*, *Gfap*, and *C1qb*) are not upregulated in very long incubation time 0/+ mice until ~16 weeks (~30% of the incubation period) when levels of PrP^{Sc} were first detectable in histoblots. Increased levels of these glial mRNAs occurred earlier (12 weeks) but after a greater portion of the 54% of incubation time had passed in their short incubation time partner (Figure 3B). The appearance of glial DEGs in 0/+ mice well before any clinical signs or increase in the expression of genes indicative of neuronal damage implicates a direct response to PrP^{Sc}, though signals from neurons can be ruled out.

Tg4053 mice have a short interval from inoculation to death and in conjunction with 0/+ mice could aid in discrimination of replication and pathogenesis. RML-infected Tg4053 mice overexpressing PrP showed significant changes in 125 ($P<0.05$ in Tg4053) of the 333 DEGs in the shared set. Prominent shared DEGs in most of the key shared modules exhibited similar patterns in Tg4053 mice, though generally with differentials of smaller magnitude and closer in time to clinical illness and death than all other combinations of prion and strain (see Figure 3). Tg4053 mice also showed a set of highly significant DEGs that were not seen in the other combinations. The 20 DEGs that were most significant in Tg4053 mice along with their expression in the other combinations are shown in Figure 2C. Unlike 0/+ mice, Tg4053 mice (that overexpress PrP and die from RML scrapie at ~8 weeks) show increases in a set of glial genes at 6 weeks (75% of its incubation time; Figure 3B). The difference in dynamics of such genes is similar to the dynamics of PrP^{Sc} increase. Note the points at 16 weeks in 0/+, 12 weeks in FVB wild type, and 6 weeks in Tg4053 mice (see the arrows in Figure 3A histoblots). Also we noted that the temporal patterns of such genes are similar to those of the genes involved in androgen/arachidonate metabolism and synaptic upregulated DEGs. Combining the observations in Figure 3, we conclude that microglial activation and reactive astrocytic gliosis reflect responses to accumulation of PrP^{Sc} as well as to early degenerative changes in neurons, specifically synapse loss (Jeffrey *et al*, 2000; Ishikura *et al*, 2005). Note that DEGs associated with neurodegenerative changes are not detected in our whole-brain data until disease is widespread.

Construction of dynamic networks: PrP^{Sc} accumulation

To associate the genes showing differential expression patterns with fundamental processes, we constructed hypothetical dynamic networks. Of the 333 shared DEGs, only 173 genes had sufficient protein–protein interaction or metabolic pathway information available in the literature for inclusion in one or more of our networks; 161 of these genes were included. Among the 161 'network' genes, 117 genes were mapped to functional modules that have been previously associated with prion disease, whereas 44 genes were used to construct six novel functional modules (see Table II for selected genes for the novel modules; see below for details). The 172 genes that could not be so included have been grouped according to known functions (114 genes with prion-associated functions, 19 genes with novel functions, 27 genes with predicted functions, and 12 genes with no known functions; see also Supplementary Table S1 for details and Supplementary Figure S8 for distribution of the genes in the various groups) or shared temporal expression patterns (Supplementary Figure S3). Interestingly, two shared DEGs with unknown functions (*AU020206* and *2310033F14Rik*) were identified from non-coding regions of the genome. It will be interesting to characterize their possible regulatory roles, if any, in prion disease.

To produce comprehensive networks, we relaxed the stringent *P*-value cutoff of 10^{-3} that was used for shared DEGs to include more transcripts ($P<0.01$) showing similar differential expression patterns in two or more combinations. The inclusion of such genes allowed us to reconstruct well-connected networks thus describing a broad range of prion-related biological processes, which were still represented by the shared DEGs (Supplementary information). For network construction, we clustered these genes into four groups representing four major pathological features of prion disease: (1) PrP^{Sc} replication and accumulation, (2) synaptic degeneration, (3) microglial and astrocyte activation, and (4) neuronal cell death. This was done by GO clustering of the genes using FuncAssociate (Berriz *et al*, 2003) and then assigning the GO clusters to one or more of the four pathological feature groups, based on relationships between the corresponding GO terms and four pathological features (Supplementary Table S2 and Supplementary Figure S4). For example, GO clusters of chemotaxis and complement activation were assigned to microglial and astrocyte activation. When the relationships were not obvious, such GO clusters were assigned to all groups of pathological features in which the GO processes can be possibly involved. For example, complement activation was assigned to both PrP^{Sc} replication and accumulation and microglial and astrocyte activation. Using the proteins encoded by selected genes assigned to each pathological group and their nearest interacting proteins, we constructed a hypothetical protein network describing the interactions in prion-related biological processes representing each pathological feature and their dynamic transitions. The interactions among the network nodes were obtained from the interaction databases, BIND (http://www.bind.ca) and HPRD (http://hprd.org). The network nodes were localized according to GO subcellular component information (lysosome, ER, PM, ECM, and so on), and the cell types (neuron, oligodendrocyte, microglia, or astrocyte) were assigned according to information from literature and public databases. Strikingly, assignment of cell types for 128 selected DEGs verified by cell type-specific patterns from *in situ* hybridization data of B6 mouse brains and image-based informatics annotation (for detailed methods, see Lein *et al*, 2007—describing the Allen Brain

Atlas) was virtually completely consistent with the cell-type assignments in our hypothetical networks (Supplementary Table S5). Some of the nodes and modules were assigned to microglia/astrocytes as these two cell types share gene expression of major components involved in immune responses (e.g. complement, TLRs, and cytokines). The

Table II Novel functions represented by selected genes from 333 DEGs (differentially expressed genes) shared by five mouse–prion combinations

Category	Gene symbol[a]	Description	Entrez ID	Previous studies[b]	Human orthologs[c]
Leukocyte extravasation	Csf1*	Colony-stimulating factor 1 (macrophage)	12977		CSF1
	Prg1*	Proteoglycan 1, secretory granule	19073		SRGN
	Selpl*	Selectin, platelet (p-selectin) ligand	20345		SELPLG
	Cyba	Cytochrome *b*-245, alpha polypeptide	13057	R, X4	CYBA
	Itgax	Integrin alpha X	16411	R, X4	ITGAX
	Msn	Moesin	17698	R, X4	MSN
Androgen metabolism	Cyp7b1*	Cytochrome *P*450, family 7, subfamily b, polypeptide 1	13123		CYP7B1
	Hsd3b7*	Hydroxy-delta-5-steroid dehydrogenase, 3 beta- and steroid delta-isomerase 7	101502		HSD3B7
	Slco2b1*	Solute carrier organic anion transporter family, member 2b1	101488		SLCO2B1
	Bzrp	Benzodiazepine receptor, peripheral	12257	X	TSPO
	Dbi	Diazepam-binding inhibitor	13167	S, Sk, Bo	DBI
Iron homeostasis and heme metabolism	Cp*	Ceruloplasmin	12870		CP
	Hfe*	Hemochromatosis	15216		HFE
	Slc39a14*	Solute carrier family 39 (zinc transporter), member 14	213053		SLC39A14
	Ftl1	Ferritin light chain 1	14325	Sk	FTL
	Trf	Transferrin	22041	Sk, Bo	TF
Demyelination, neurogenesis, axonal transport, ion channels	*Kif5c**	Kinesin family member 5C	16574		KIF5C
	Lgi4*	Leucine-rich repeat LGI family, member 4	243914		LGI4
	Nupr1*	Nuclear protein 1	56312		NUPR1
	P2rx7*	Purinergic receptor P2X, ligand-gated ion channel, 7	18439		P2RX7
	*Scn1a**	Sodium channel, voltage-gated, type I, alpha	20265		SCN1A
Arachidonate/phospholipid metabolism and calcium signaling pathway	Alox5ap*	Arachidonate 5-lipoxygenase-activating protein	11690		ALOX5AP
	Cyp4f14*	Cytochrome *P*450, family 4, subfamily f, polypeptide 14	64385		CYP4F2
	Ptgs1*	Prostaglandin-endoperoxide synthase 1	19224		PTGS1
	Hpgd	Hydroxyprostaglandin dehydrogenase 15 (NAD)	15446	Bo, R	HPGD
	Plce1*	Phospholipase C, epsilon 1	74055		PLCE1
	Adcy7*	Adenylate cyclase 7	11513		ADCY7
Hematopoiesis	Gmfg*	Glia maturation factor, gamma	63986		GMFG
	Inpp5d	Inositol polyphosphate-5-phosphatase D	16331	X	INPP5D
	Lcp1	Lymphocyte cytosolic protein 1	18826	X4	LCP1
	Lpxn	Leupaxin	107321	X	LPXN
	Nckap1l	NCK-associated protein 1 like	105855	X	NCKAP1L

Old gene symbols[d]	Updated gene symbol	Description	Entrez ID
Bzrp	Tspo	Translocator protein	12257
Prg1	Srgn	Serglycin	19073
Selpl	Selplg	Selectin, platelet (p-selectin) ligand	20345

[a]Genes with asterisk are unique DEGs to this study; genes in bold and italic show decreased expression in infected mouse brains.
[b]S (Sorensen *et al*, 2008); X (Xiang *et al*, 2007); Sk (Skinner *et al*, 2006); Br (Brown *et al*, 2005); Bo (Booth *et al*, 2004); R (Riemer *et al*, 2004); X4 (Xiang *et al*, 2004).
[c]Orthologous human gene symbols are current as of 28 August 2008.
[d]Gene symbols have been updated in the EntrezGene database as of 28 August 2008.

Figure 4 Dynamic PrP replication and accumulation network. Hypothetical networks of proteins and metabolites that are potentially involved in PrP replication and accumulation were constructed starting from the list of 333 shared DEGs and protein–protein interaction/metabolic pathway information from public databases. Relative changes of the transcripts for the corresponding proteins are represented in color changes: red—upregulation, green—downregulation, yellow—no change. Data for the transcriptional changes are from BL6 mice infected with RML prions, at 6 weeks (**A**), 10 weeks (**B**), 14 weeks (**C**), 18 weeks (**D**), 20 weeks (**E**), and 22 weeks (**F**) after inoculation. See main text for detailed description of modules 1 through 6. Ch: cholesterol; ECM: extracellular matrix; PM: plasma membrane. Large nodes indicate DEGs whose expression change patterns are shared by five prion–mouse combinations (B6-RML, B6-301V, B6.I-RML, B6.I-301V, and FVB-RML); asterisks indicate DEGs whose prion-related changes are unique in this study; genes in blue are also DEGs in RML-infected 0/+ mice; genes in bold are also DEGs in RML-infected Tg4053 mice; genes with solid underline were changed only in mice with short incubation times; genes with dotted underline were changed only in RML-infected mice. Source data is available for this figure at www.nature.com/msb.

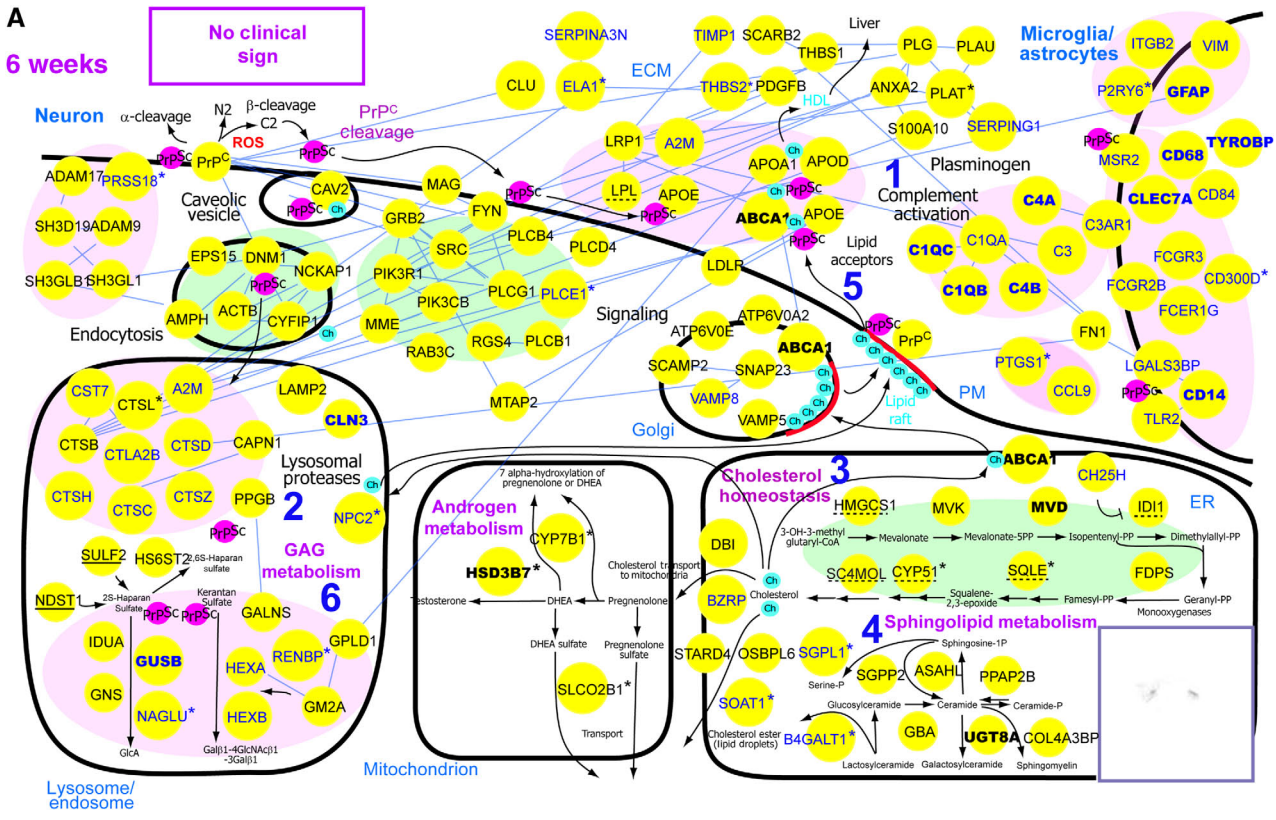

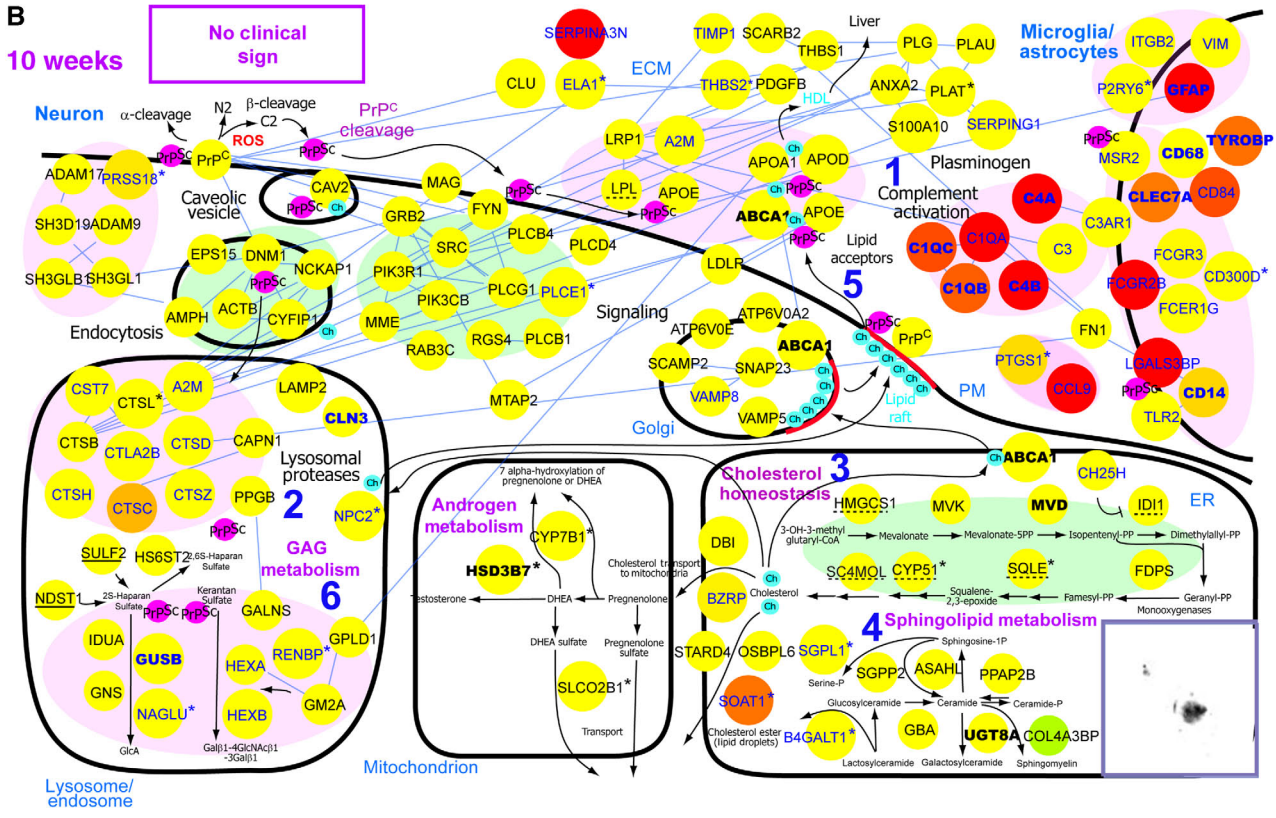

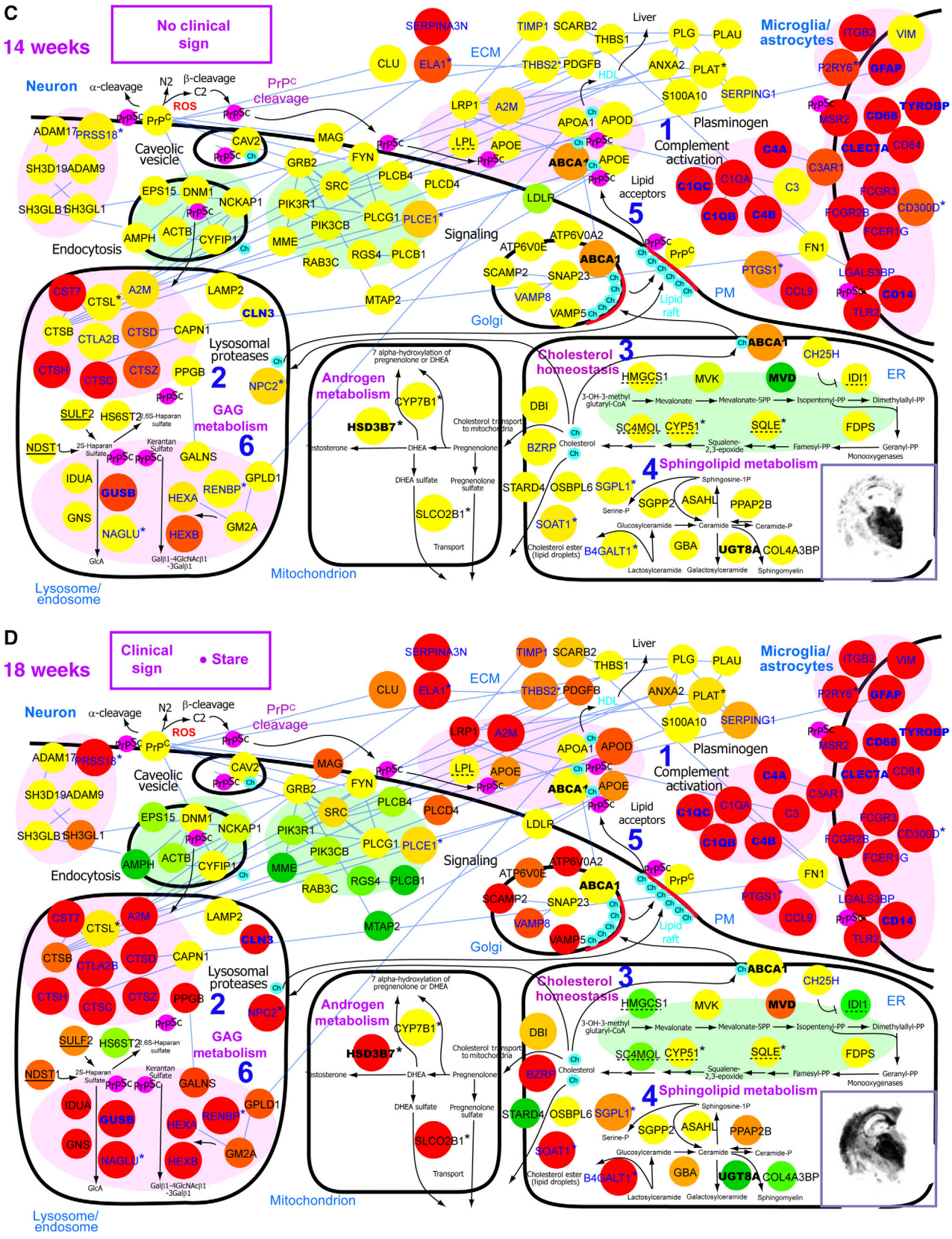

Figure 4 Continued.

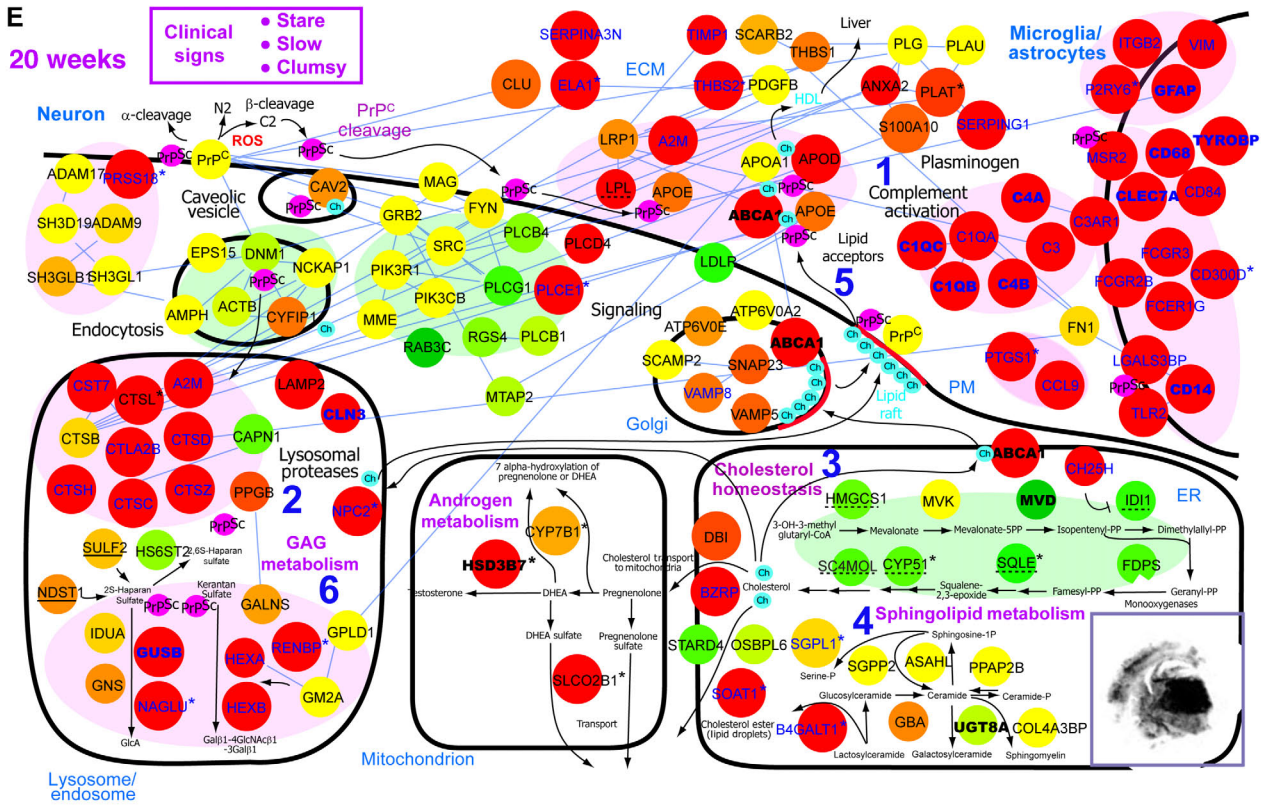

Figure 4 Continued.

protein node colors represent the increase (red) and decrease (green) in the expression of the corresponding genes at each time point in B6 mice inoculated with RML. The nodes were then clustered into functional network modules based on the similarity in their GO biological processes and their connectivity (Hwang *et al*, 2005) (see Supplementary Table S2 for details). The arrows representing metabolic and signaling pathways were also added based on the KEGG pathways. As an example, a network of interacting proteins hypothesized to be involved in prion replication or responses to PrP^{Sc} accumulation is presented in Figure 4 with the dynamic changes in gene expression in B6-RML shown at 6, 10, 14, 18, 20, and 22 weeks. The highly significant ($P<10^{-3}$) DEGs are indicated by larger sized nodes, and DEGs unique to this study are indicated by asterisks. The underlined nodes represent the genes upregulated only in mice with short incubation times, and the dotted-underlined nodes represent the genes differentially expressed only in mice infected by RML prions. A histoblot showing distribution of proteinase K-resistant PrP^{Sc} in coronal sections including the hippocampal formation (approximately Bregma −1.5 to −2.2 mm) is included in each time point panel along with notation of clinical signs. All data collected in this study are available online (http://prion.systemsbiology.net/). It is important to emphasize that the networks discussed here are hypothetical and construction of alternatives using other methods is encouraged.

The network transitions show that dynamic perturbations of gene expression associated with biological processes occur in a specific order, which independently verifies the conclusion that neuropathological changes proceed in a stereotypical set of steps (Bouzamondo-Bernstein *et al*, 2004). Among the first detectable expression changes (10 weeks) were increases in mRNA levels of *C1qa/b* and *C3ar1* reflecting activation of microglia and astrocytes, one of the earliest detectable responses to prion infection (Klein *et al*, 2001) (Figure 4B, module 1). Around the same time, the increased activities of lysosomal proteases were suggested by elevation of the lysosomal protease gene *Ctsc* (Figure 4B, module 2): lysosomal proteases may have a role in degradation as well as formation of PrP^{Sc} (Zhang *et al*, 2003). Changes within the lysosomal module became more obvious at later time points (Figure 4C, module 2). The network also shows dysregulation associated with the synthesis, trafficking, and processing of cholesterol and sphingomyelin, two of the major components of lipid rafts where the initial steps of PrP^{Sc} replication are thought to occur (Simons and Ehehalt, 2002). At 10 weeks, changes were detected in the expression of genes controlling trafficking and conversion of cholesterol (Figure 4B, module 3) and sphingomyelin (Figure 4B, module 4) (Rodriguez-Agudo *et al*, 2008). At 14 weeks, expression levels of cholesterol synthesis genes, such as *Mvk* and *Mvd*, were decreased, but expression of the cholesterol transporters or acceptors including *Abca1*, *A2m*, and *Apod* were increased (see the arrows in Figure 4C, module 5). As will be discussed later, decreases in the expression of genes involved in cholesterol biosynthesis are particularly pronounced in mice infected with the RML prion strain.

Changes in sphingolipid metabolism, potentially leading to a decrease in galactosylceramide, which is found in PrP^{Sc} deposits (Klein *et al*, 1998), are evident by 18 weeks (Figure 4D, module 4). The network also shows an increase in GAG metabolism, indicated by increased *Gusb* and *Hexb* mRNA levels, first detectable at 14 weeks (Figure 4C, module 6) (Mayer-Sonnenfeld *et al*, 2005). This dynamic coupling of cholesterol, GAG, and sphingolipid pathways with PrP^{Sc} suggests, together with the findings from previous studies, that prion replication requires the close physical association among PrP^{C}/PrP^{Sc}, GAG, cholesterol, and sphingolipid on lipid rafts in the plasma membrane and during trafficking to the lysosome and endosome (Hijazi *et al*, 2005; Horonchik *et al*, 2005). Novel therapeutic approaches for prion disease can be developed that target these components simultaneously (see Discussion for details).

Dynamic network describing microglial/astrocytic activation

Similar to most infectious agents, PrP^{Sc} induces inflammatory responses by activating innate immunity through glial cells (microglia and astrocytes) in the brain (Perry *et al*, 2002; Sorensen *et al*, 2008). We constructed a protein network model using the shared DEGs that are associated with microglial/astrocytic activation (Figure 5). This is consistent with neuropathological data showing that microglia are among the earliest responders to any form of neurodegeneration (Rezaie and Lantos, 2001; Wojtera *et al*, 2005), that microglia proliferate and hypertrophy in prion disease in response to deposition of PrP^{Sc} (Williams *et al*, 1997), and that reactive astrocytic gliosis, which tends to follow activation of microglia, is induced by factors released from microglia (Jensen *et al*, 1994; Ohno *et al*, 1995; Nakamura, 2002; Panickar and Norenberg, 2005). Transcriptome analysis suggests that the first apparent reactive changes (from 10 weeks in B6-RML) are activation of complement pathways by PrP^{Sc} (Klein *et al*, 2001; Sim *et al*, 2007; Figure 5, module A), pattern recognition receptors (PRRs), and other receptors potentially responsible for PrP^{Sc} recognition and uptake (Figure 5, module B). Lack of increased expression of innate immune system genes in 0/+ mice before 16–18 weeks is compatible with gliosis and expression of these genes in glia rather than neurons as it appears that little neuronal damage is seen at this stage (Figure 5). Similarly, the kinetics of expression of innate immune receptors and their downstream cytokines relative to PrP^{Sc} accumulation suggest that these receptors may recognize proteins perturbed by prion infection, such as intraneuronal proteins and peptides released as a result of early synaptic changes, rather than carbohydrate moieties on PrP^{Sc}. Complement complexes and PRRs may be responsible for stimulating the production of cytokines, chemokines (Figure 5, module C), and growth factors (Figure 5, module D), as well as for astrocytic activation as indicated by increased expression of glial markers such as *Gfap* and P2RY receptors (Wang *et al*, 2005; Figure 5, module E). Activation of endothelial cells through cytokines released from microglia and astrocytes would enhance migration of leukocytes from the blood and their differentiation into microglia (Figure 5, module F). This possibility is supported by the increased expression of genes involved in the multistep processes of leukocyte extravasation: selectin ligands, adhesion molecules, chemokines and their receptors, integrins, transendothelial migration genes, and intracellular signaling molecules. Conversion of mononuclear

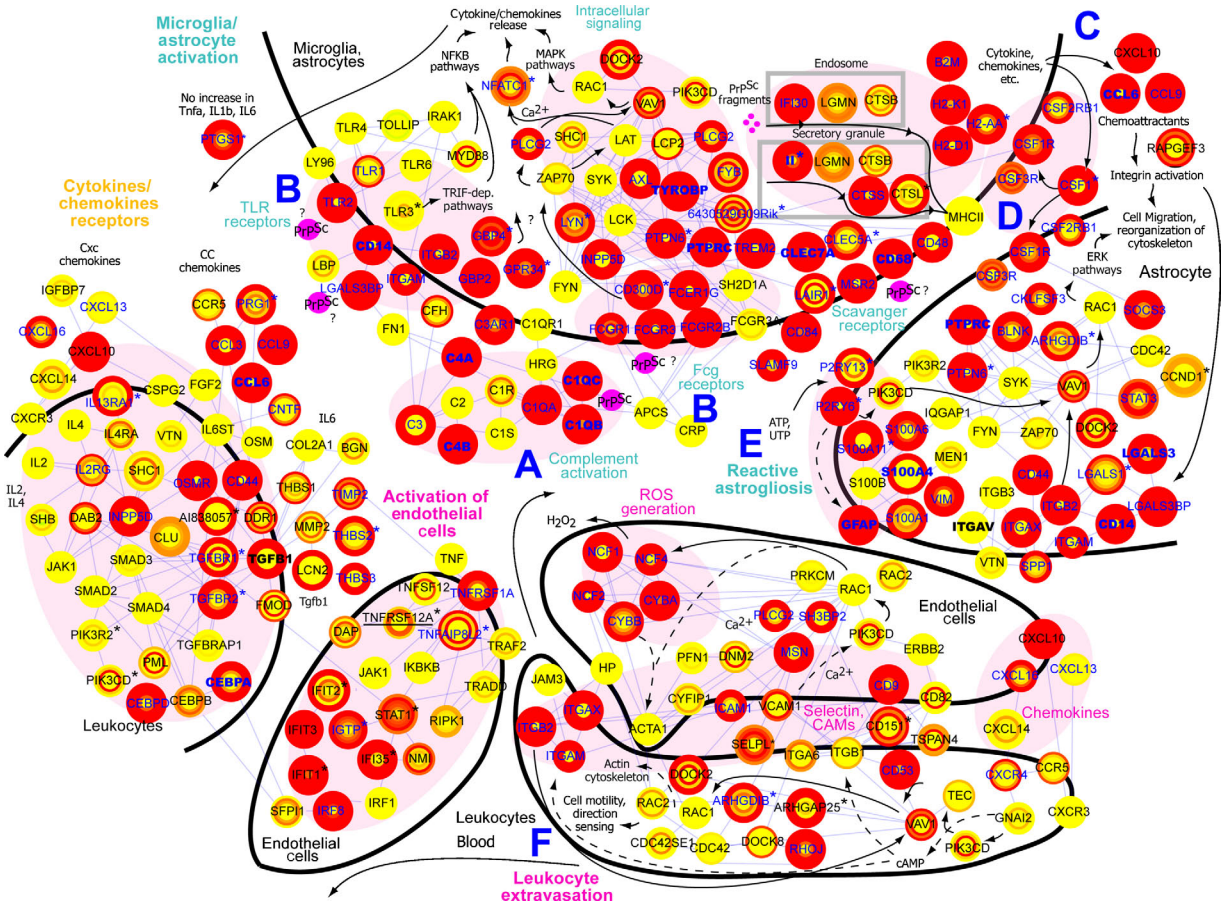

Figure 5 Microglial and astrocyte activation network. Hypothetical networks of proteins and metabolites that are potentially involved in activation of microglia and astrocytes were constructed starting from the list of 333 shared DEGs and protein–protein interaction information from public databases. Modules A–F denote distinct functional modules within the network: (A) Complement activation, (B) pattern recognition receptors, (C) cytokines and chemokines, (D) growth factors, (E) reactive astrogliosis, and (F) leukocyte extravasation. Relative changes of the transcripts for the corresponding proteins are represented in color changes: red—upregulation, green—downregulation, yellow—no change. Data for differential expression are from BL6 mice infected with RML prions. The temporal expression changes at six time points (10, 14, 16, 18, 20, and 22 weeks) are represented by the circular heatmaps of the network nodes: the center color of each node indicates the differential expression at 10 weeks, while the outer circle colors represent expression changes at increasing time points. Large nodes indicate DEGs whose expression change patterns are shared by five prion-mouse combinations; asterisks indicate DEGs whose prion-related changes are unique in this study; genes in blue are also DEGs in RML-infected 0/+ mice; genes in bold are also DEGs in RML-infected Tg4053 mice; genes with solid underline were changed only in mice with short incubation times. Source data is available for this figure at www.nature.com/msb.

leukocytes (blood monocytes) into microglia when they enter the brain is suggested by upregulation of *Csf1* (Figure 5, module D). Most of these DEGs were shared by 0/+-RML mice, thus implying their potential importance in PrP^{Sc} replication, but indicating that these responses on their own are insufficient for the production of clinical signs. Although this might reflect a response to more rapidly accumulating PrP^{Sc}, recruitment of microglial cells from blood also might facilitate PrP^{Sc} replication by increasing PrP^{Sc} trapping.

Networks highlighting neurodegeneration and cell death were also constructed and are presented and discussed as Supplementary Figures S5 and S6 and are presented on the PDDB website.

Novel network modules

Our strategy identified many shared genes not previously associated with prion disease. Examining the recent literature for metabolic pathways in which these genes are involved, in conjunction with the similarity of their expression profiles, led us to hypothesize several novel modules with concerted changes of expression for closely related genes. The androgen metabolism module is illustrated in Figure 6A. To our knowledge, this is the first report of potential involvement of androgen metabolism in prion disease. BZRP (translocator protein, 18 kDa) functions as an essential rate-limiting step toward mitochondrial biosynthesis of androgenic molecules, together with its endogenous ligand diazepam-binding inhibitor (*Dbi*) (Papadopoulos and Brown, 1995; Papadopoulos *et al*, 2006). The global stimulation of androgen biosynthesis pathway implies altered levels of neurosteroids in prion disease. In addition, the increased expression of *Cntf* as shown here and in a previous study (Na *et al*, 2007) may suggest a link between perturbed androgen metabolism and glial activation in prion-infected brains as *Cntf* upregulation leads to reactive astrogliosis through the JAK/STAT pathway. A possible

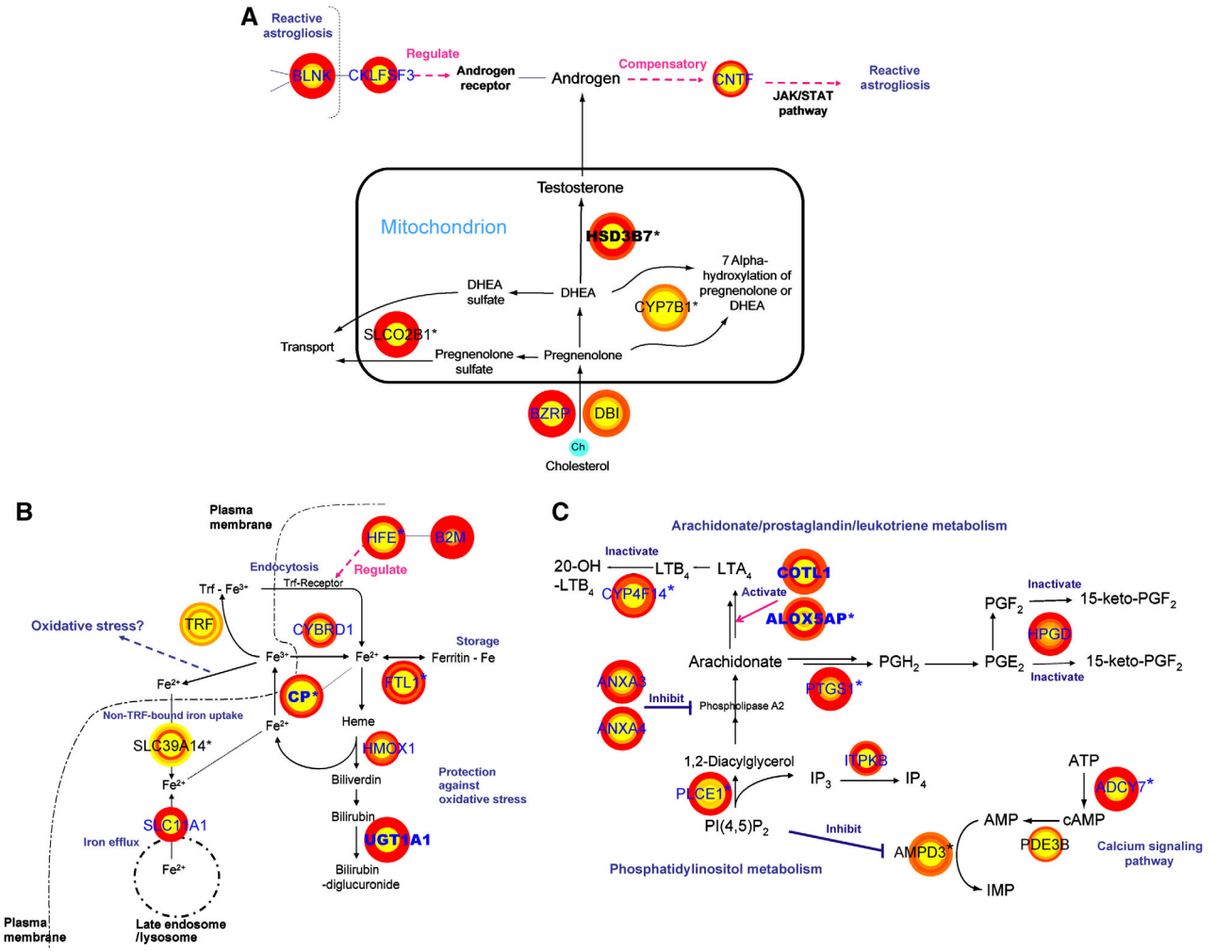

Figure 6 Novel functional modules with dynamic gene expression changes potentially linked to prion pathophysiology: (**A**) androgen metabolism, (**B**) iron metabolism, (**C**) arachidonate/phospholipid metabolism. Hypothetical networks of proteins and metabolites that are potentially involved in three novel functional modules were constructed based on genes selected from the list of 333 shared DEGs and metabolic pathway information from literature. The temporal expression changes at six time points (10, 14, 16, 18, 20, and 22 weeks after inoculating BL6 mice with RML prions) are represented by the circular heatmaps of the network nodes: the center color of each node indicates the differential expression at 10 weeks, whereas the outer circle colors represent expression changes at increasing time points. Large nodes indicate DEGs whose expression change patterns are shared by five mouse-prion combinations; asterisks indicate DEGs whose prion-related changes are unique in this study. See text for detailed description of the three pathways.

regulatory relationship between CKLFSF3 and androgen receptor has recently been reported (Wang *et al*, 2008). CKLFSF3 interacts directly with BLNK (Imamura *et al*, 2004), further suggesting a tie between androgen metabolism and glial activation (see Figure 5, module E). The temporal patterns of these genes were similar to those in cholesterol clearance (Figure 3B and Figures 4D–F, module 3), implying that dysregulated cholesterol metabolism also may be coupled to the perturbation of neurosteroid metabolism.

A second module with potential importance in prion disease involves iron homeostasis and heme metabolism. Concurrent upregulation was detected for genes involved in iron uptake, transport, storage, and heme degradation (Figure 6B). These results are consistent with two recent *in vivo* observations: (1) increased levels of redox-active iron in scrapie-infected mouse brain (Kim *et al*, 2000; Basu *et al*, 2007) and (2) a stimulatory effect of redox iron on the conversion of PrP^{C} to PrP^{Sc} (Basu *et al*, 2007). The activation of the heme degradation pathway in the brain has been associated with cellular response to oxidative stress (Baranano *et al*, 2002). Six DEGs (*Mgst1*, *Mt1*, *Mt2*, *Prdx6*, *Scara3*, and *Ucp2*) with protective functions against oxidative stress showed patterns of expression similar to those of iron heme metabolism genes, suggesting interaction between the two modules (data not shown). Iron homeostasis is essential for the maintenance of oligodendrocytes and myelin in brain (Connor and Menzies, 1996; Ortiz *et al*, 2004), and its dysregulation may be related to demyelination in prion disease (Walis *et al*, 2004; Baumann *et al*, 2007). Indeed, our data show significant changes in the expression of genes encoding proteins involved in myelination (*Padi2*, *AI838057/Met*, and *Nupr1* (Plant *et al*, 2006; Moscarello *et al*, 2007; Ohya *et al*, 2007).

A third module of interest from our data is arachidonate/prostaglandin metabolism, in conjunction with phospholipid metabolism and calcium signaling pathway. Shared DEGs that are involved in biosynthesis of proinflammatory prostaglandins

Table III Functions predicted for selected genes from 333 DEGs shared by five mouse–prion combinations

Category	Gene symbol[a]	Description	Entrez ID	Previous studies[b]	Human orthologs[c]
Protection against oxidative stress	Naprt1*	Nicotinate phosphoribosyltransferase domain containing 1	223646		NAPRT1
Arachidonate/phospholipid metabolism	Bmp2k*	BMP2-inducible kinase	140780		BMP2K
	E030018N11Rik*	RIKEN cDNA E030018N11 gene	319622		ITPRIPL2
Hematopoiesis	Pbxip1*	Pre-B-cell leukemia transcription factor interacting protein 1	229534		PBXIP1
Chondrogenesis	Loh11cr2a*	Loss of heterozygosity, 11, chromosomal region 2, gene A homolog (human)	67776		VWA5A
Complement system (coagulation)	Pp11r*	Placental protein 11 related	19011		P11
	BC032204	cDNA sequence BC032204	108101	X, X4	FERMT3
Interferon-related	Aldh1l2*	Aldehyde dehydrogenase 1 family, member L2	216188		ALDH1L2
	D12Ertd647e*	DNA segment, Chr 12, ERATO Doi 647, expressed	52668		NA
	Plscr2*	Phospholipid scramblase 2	18828		PLSCR2
Other immune response genes	4632428N05Rik*	RIKEN cDNA 4632428N05 gene	74048		C10orf54
	Stno*	Strawberry notch homolog (Drosophila)	216161		SBNO2
	Gp49a	Glycoprotein 49 A	14727	X, R	NA
Metal ion binding	Antxr1*	Anthrax toxin receptor 1	69538		ANTXR1
	Dtx3l*	Deltex 3-like (*Drosophila*)	209200		DTX3L
	Eya4*	Eyes absent 4 homolog (*Drosophila*)	14051		EYA4
Membrane trafficking	Crispld2*	Cysteine-rich secretory protein LCCL domain containing 2	78892		CRISPLD2
Signal transduction	4933428I03Rik*	RIKEN cDNA 4933428I03 gene	66775		PTPLAD2
Nucleic acid binding	Scrg1	Scrapie responsive gene 1	20284	DD	SCRG1
DNA damage repair	Parp12*	Poly (ADP-ribose) polymerase family, member 12	243771		PARP12
Guanylate binding	Mpa2l*	Macrophage activation 2 like	100702		NA
Neurological disorder related	0610011I04Rik*	RIKEN cDNA 0610011I04 gene	66058		TMEM176A
	1810009M01Rik*	RIKEN cDNA 1810009M01 gene	65963		TMEM176B
	Phyhd1*	Phytanoyl-CoA dioxygenase domain containing 1	227696		PHYHD1
Non-coding genes	AU020206	Expressed sequence AU020206	101757	X4	NA
	2310033F14Rik*	RIKEN cDNA 2310033F14 gene	69555		NA
No predicted functions	1810059G22Rik*	RIKEN cDNA 1810059G22 gene	67706		TMEM179B
	2310014H01Rik*	RIKEN cDNA 2310014H01 gene	76448		KIAA1949
	*4933411K20Rik**	RIKEN cDNA 4933411K20 gene	66756		KIAA1430
	9230105E10Rik*	RIKEN full-length enriched library, clone: A130050C20 product	245575		NA
	A530050D06Rik*	RIKEN cDNA A530050D06 gene	104816		LOC374569
	AI452102*	Expressed sequence AI452102	330594		NA
	E230029C05Rik*	RIKEN cDNA E230029C05 gene	319711		NA
	2810459M11Rik	RIKEN cDNA 2810459M11 gene	72792	X	C2orf72
	BC025600	cDNA sequence BC025600	231633	X, Sk	TMEM119
	X99384	cDNA sequence X99384	27355	X	KIAA1274

Old gene symbols[d]	Updated gene symbol	Description	Entrez ID	Comments
0610011I04Rik	Tmem176a	Transmembrane protein 176A	66058	
1810009M01Rik	Tmem176b	Transmembrane protein 176B	65963	
1810059G22Rik	Tmem179b	Transmembrane protein 179B	67706	
4933428I03Rik	Ptplad2	Protein tyrosine phosphatase-like A domain containing 2	66775	
AI452102	E230029C05Rik	RIKEN cDNA E230029C05 gene	330594	New GeneID: 319711
BC025600	Tmem119	Transmembrane protein 119	231633	
BC032204	Fermt3	Fermitin family homolog 3	108101	
Cklfsf6	Cmtm6	CKLF-like MARVEL transmembrane domain containing 6	67213	
Loh11cr2a	Vwa5a	von Willebrand factor A domain containing 5A	67776	
Stno	Sbno2	Strawberry notch homolog 2	216161	

[a]Genes with asterisk are unique DEGs to this study; gene in bold and italic shows decreased expression in infected mouse brains.
[b]X (Xiang *et al*, 2007); Sk (Skinner *et al*, 2006); R (Riemer *et al*, 2004); X4 (Xiang *et al*, 2004); DD (Dandoy-Dron *et al*, 1998).
[c]Orthologous human gene symbols are current as of 28 August 2008. Those denoted as 'NA' do not have official orthologous human genes.
[d]Gene symbols of the following 10 genes have been updated in the EntrezGene database as of 28 August 2008.

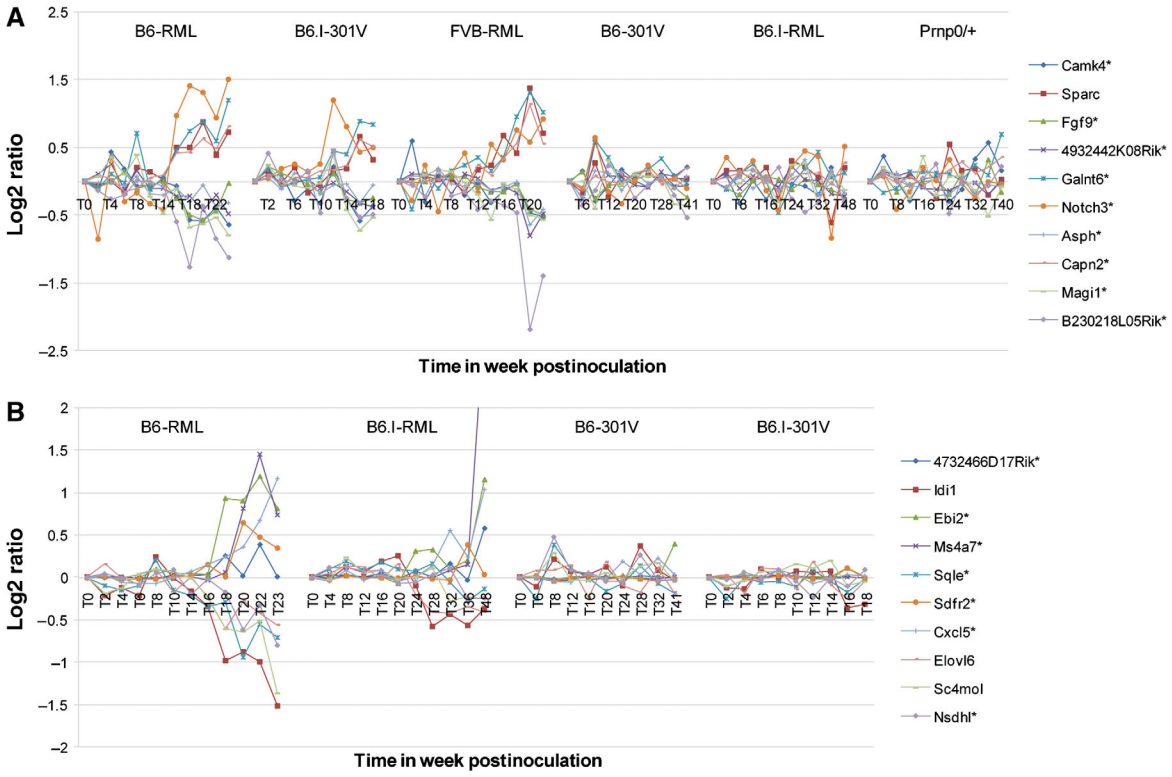

Figure 7 Expression profiles of DEGs changing predominantly in three short incubation time combinations or in two RML-infected mice. (**A**) Top 10 genes that show selective changes in short incubation time combinations, B6-RML, B6.I-301V, and FVB-RML as compared with long incubation time combinations (B6-301V and B6.I-RML). The changes of these genes in 0/+ is also shown as another example of mouse–prion combination with long incubation time; (**B**) top 10 genes that show selective changes in RML-infected combinations, B6-RML and B6.I-RML as compared with 301V-infected combinations, B6-301V and B6.I-301V.

and leukotrienes from arachidonate and their clearance show shared patterns of increased expression (Figure 6C). Activation of this module should prompt a search for excessive production of these pro-inflammatory metabolites in prion-infected brains (Kikuta *et al*, 2000). Interestingly, upregulation of COX-1 (*Ptgs1*) has been observed in post-mortem brains of CJD patients (Deininger *et al*, 2003). Moreover, it was recently shown that coactosin-like 1 (*Cotl1*) can also upregulate ALOX5 (5-lipoxygenase) activity and LTA_4 production in a Ca^{2+}-dependent manner (Rakonjac *et al*, 2006). Changes in arachidonate metabolism may be linked with the perturbation of phosphatidylinositol metabolism and calcium signaling pathway through AMP deaminase (Figure 6C).

Five additional processes (demyelination-neurogenesis, hematopoiesis, chondrogenesis, DNA damage repair, and uracil/thymidine catabolism), represented by 20 shared DEGs, may also be associated with prion disease (see Table II for selected modules and genes and Supplementary Table S1 for the complete list). In addition, among 39 DEGs with no known functions, 27 genes can be potentially related to various functional modules mentioned above through predictions using protein domain information or indirect experimental evidence (for example, *E030018N11Rik* is predicted to be involved in phospholipid metabolism because of its protein sequence similarity to ITPRIP family, including inositol 1,4,5-triphosphate receptor interacting protein; see Table III for truncated list of predicted functions and associated genes and Supplementary Table S1 for the complete list).

In short, novel associations revealed in our study can be used to generate testable hypotheses for events in prion disease. Searching for associations among subgroups of mouse strain–prion strain combinations is also worthwhile. The complete list of functional modules enriched with 333 shared DEGs is shown in Supplementary Table S1.

Incubation time- and prion strain-associated DEGs

Grouping mice according to differences in incubation times among the five core prion–mouse combinations that were used to define shared DEGs identified 55 genes, the expression of which was significantly increased ($P<10^{-4}$) in the three short incubation time combinations (B6-RML, B6.I-301V, and FVB-RML) but showed no significant change in mice with long incubation times (B6-301V and B6.I-RML). Statistical methodologies for grouping DEGs by incubation time or prion strain are provided in Supplementary information. Examples are shown in Figure 7. In total, 27 of these short incubation time DEGs showed increased expression in scrapie-infected mice and 28 were downregulated (Supplementary Table S3). There were no genes that were differentially expressed only in the long incubation time combinations. It is important to stress that a long incubation time in itself does not preclude detecting differential expression of the short incubation time DEGs. RML-infected 0/+ mice, which have very long incubation times, show significant scrapie-induced changes in 5 of the 55 'short incubation time' DEGs ($P<0.05$ in 0/+-RML). Among

the 55 genes showing differential expression in short incubation time combinations, we found decreased expression of four genes (*Cycs*, *Ndufa10*, *Cox6b1*, and *Atp5j2*) involved in ATP biosynthesis in the oxidative phosphorylation pathway (Supplementary Figure S7A), and increased expression of five genes (*Chst2*, *Ndst1*, *Sdc3*, *Sulf2*, and *Galnt6*) that mediate biosynthesis of various GAGs (Figure 4, see also Supplementary Figure S7B). The increased levels of *Ndst1* and *Sulf2* and decreased expression of *Hs6st2*, whose protein catalyzes the 6-O-sulfation of heparan sulfates (a function opposite to that of SULF2) may redirect metabolic flux to 2-O-sulfated heparan sulfate, an entry point to the GAG degradation pathway (Pikas *et al*, 1998). This finding is consistent with the potential roles of GAG in prion pathology as membrane receptors for PrP^{Sc} as noted earlier and is supported by the effect of drugs interfering with PrP^{Sc}–GAG interactions, such as Tilorone (Mayer-Sonnenfeld *et al*, 2008) and Copaxone (Engelstein *et al*, 2007) on increasing the incubation time of prion disease. It is important to stress that the differences between short and long incubation time DEGs are not absolute, but rather quantitative differences in expression between the two groups. Thus, our data suggest that perturbation of mitochondrial ATP synthesis and lysosomal GAG biosynthesis are two important factors that can contribute to accelerated progression of prion disease. We also found that the remaining 55 short incubation time DEGs are involved in various signaling pathways such as calcium signaling (e.g. *Camk4*), phosphatidylinositol signaling (e.g. *Itpr1*), and MAPK signaling pathways (e.g. *Ptprr*) as well as in adhesion (e.g. *Pvrl3*), axon guidance (e.g. *Ntng1*), and apoptosis (e.g. *Cflar*).

Grouping the B6 and B6.I congenic strains according to prion strain identified 39 DEGs that were significant only in RML inoculated mice. In total, 19 of these genes were elevated and 20 showed decreased expression. These genes are indicated in Supplementary Table S4 and Figure 7. No DEGs were found that were specific to 301V inoculated mice. Interestingly, 7 of the 20 genes with decreased expression (*Hmgcs1*, *Nsdhl*, *Cyp51*, *Sc4mol*, *Idi1*, *Sc5d* and *Sqle*) are involved in cholesterol biosynthesis, showing consistent reduction in RML-infected mice but no significant changes in 301V-infected mice (Figure 4, module 3). Four of these genes, *Cyp51*, *Sc4mol*, *Nsdhl*, and *Sqle* show similar expression patterns in normal B6 mouse brain as assessed using the NeuroBlast function of the Allen Brain Atlas (Lein *et al*, 2007). The correlation in distribution among the four was particularly strong in the thalamus (for coronal sections, correlation coefficients with *Cyp51* for *Sqle*=0.85, for *Sc4mol*=0.76, and for *Nsdhl*=0.81).

Discussion

Our goal in using whole-brain mRNA expression data from diverse mouse strain–prion strain combinations as the core of a systems analysis of prion disease was to identify and assign function to interacting networks involved in prion replication and pathogenesis. The earliest detectable neuropathological events following intracerebral inoculation with prions are conversion of PrP^{C} to PrP^{Sc} in neuronal membranes, axonal transport of PrP^{Sc} to adjacent neurons, accumulation of PrP^{Sc} in axon terminals, and transynaptic spread of PrP^{Sc} formation in the plasma membrane of the postsynaptic neurons. Accumulation of PrP^{Sc} in synaptosomes is followed within a week by abnormal distribution of synaptic vesicles in presynaptic boutons, decreased evoked release of neurotransmitters by synaptosomes (Bouzamondo-Bernstein *et al*, 2004), presynaptic bouton degeneration and both atrophy and loss of dendrites (Ishikura *et al*, 2005). These neurodegenerative events can be highly localized early in disease, but, in combination with the resulting release of PrP^{Sc} into the extracellular space diseased cells appear to attract and activate microglia, the first responders to neurodegeneration (Rezaie and Lantos, 2001). Activated microglia may be a major factor causing nerve death in prion diseases (Giese *et al*, 1998; Priller *et al*, 2006). Although the mechanism of microglial-mediated nerve cell death is not fully understood, one possibility is overactivation of microglia secondary to exposure to PrP^{Sc} (Block *et al*, 2007).

The mechanism of nerve cell death is unknown; however, multiple pathogenic mechanisms have been proposed, including: (1) deafferentiation secondary to extensive axon terminal degeneration (Brown *et al*, 1997; Brown, 2001); (2) decreased binding affinity of receptors for neurotransmitters and trophic factors required for neuronal viability secondary to accumulation of large amounts of PrP^{Sc} in neuronal plasma membranes (Kristensson *et al*, 1993; Vey *et al*, 1996; Wong *et al*, 1996); and (3) selective degeneration of GABAergic inhibitory inputs to neurons leading to excitatory neurotoxic nerve cell death (Guentchev *et al*, 1997, 1998, 1999). Of these putative mechanisms, the continuous conversion of PrP^{C} to PrP^{Sc} in cholesterol-rich membrane rafts followed by continuous endocytosis and accumulation of large amounts of protease-resistant PrP^{Sc} in lysosomes when large numbers of neurons degenerate (Bouzamondo *et al*, 2000; Bouzamondo-Bernstein *et al*, 2004) most likely accounts for a significant amount of nerve cell death. However, these putative causes of neuronal death are not mutually exclusive and, indeed, may all contribute to late stage nerve cell death both in prion disease acquired by infection with prions and spontaneous (sporadic) and familial prion disease.

What does this brief review of our understanding of neurodegeneration in CJD and scrapie tell us? First, neurodegeneration proceeds in a stereotypical set of steps from accumulation of PrP^{Sc} in cholesterol-rich lipid rafts to early synapse degeneration to nerve cell death. Second, the data supporting such degeneration sequence are derived from research in multiple laboratories that have viewed neurodegeneration in prion diseases from different perspectives and with different preconceptions about neurodegeneration in prion disease. Our comprehensive and independent systems analysis provides gene expression that correlates very well with pathological information in the whole-brain studies of prion disease and may aid in organizing the current abundance of data fragments into a coherent pathogenic model of neurodegeneration. The meshing of our networks constructed using transcriptome data with defined pathological processes increases our confidence that systems analyses provide a valid tool for hypothesis development.

The most important feature of the dynamic networks is that the transitions in gene expression precede clinical signs and

PrP^{Sc} accumulation. For example, perturbations of several network modules, such as complement activation (Figure 4, module 1), lysosomal protease activity (Figure 4, module 2), and GAG metabolism (Figure 4, module 6) are evident earlier than the clinical signs and widespread PrP^{Sc} accumulation. It is also important to stress that changes reflecting early synaptic loss that is first detectable histologically in the thalamus are not detected until later in mRNA prepared from whole brain due to signal dilution. The dynamic changes in each of these perturbed network modules precede, but track perfectly with, clinical signs and PrP^{Sc} accumulation, indicating that the perturbations of biological processes in the network modules are potential contributors to PrP^{Sc} accumulation and the resulting clinical signs. It should be noted that virtually all neuropathological, pathophysiological and clinical data to date have been correlated with protease-resistant $rPrP^{Sc}$ and have not taken into account protease-sensitive $sPrP^{Sc}$. In the early stages of infection of mice with prions, ~80% of the total PrP^{Sc} is $sPrP^{Sc}$ (Safar *et al*, 2005). At ~60 days postinoculation (d.p.i.) when early occurring dendritic atrophy begins, about twice as much $sPrP^{Sc}$ is found in the brain than $rPrP^{Sc}$. Whether or not $sPrP^{Sc}$ perturbs biological processes presented in our hypothetical protein networks remains to be determined.

Examination of co-expression patterns can lead to development of testable hypotheses for networks important for prion pathogenesis. Our results suggest that delay or inhibition of prion replication and accumulation might be achieved by targeting some combinations of cholesterol homeostasis, GAG metabolism, and/or sphingolipid metabolism (Figure 4). Several drugs can inhibit prion replication, all of which target a biological process involved in one of these three network modules: (1) GAG depletion (chlorate, heparinase III) (Gabizon *et al*, 1993; Ben-Zaken *et al*, 2003); (2) inhibition of GAG's binding to PrP^{C} (quinacrine) (Mayer-Sonnenfeld *et al*, 2008); (3) disruption of lipid rafts through cholesterol redistribution (quinacrine) (Klingenstein *et al*, 2006) and (4) inhibition of cholesterol biosynthesis (desipramine) (Klingenstein *et al*, 2006). However, our systems approach that builds hypothetical dynamic relationships among these biological modules involved in prion replication delineates their temporal coupling. We predict that for more efficient inhibition of prion replication, GAG-, cholesterol- and sphingolipid-related processes should be targeted simultaneously. In support of this prediction, a cocktail of a synthetic chimerical compound (quinacrine + desipramine) for disruption of lipid rafts together with simvastatin for inhibition of cholesterol synthesis was reported to synergistically increase anti-prion activity (Klingenstein *et al*, 2006).

Perturbations of pathways more prominent with one prion strain than another also might provide clues on mechanisms of targeting to specific regions of the brain or cofactors involved in the conversion of PrP^{C} to PrP^{Sc}. For example, examination of DEGs prominent in short incubation time strains revealed a decreased expression for genes involved in ATP biosynthesis in the oxidative phosphorylation pathway and increased expression of GAG biosynthetic genes. Expression of genes involved in cholesterol biosynthesis was significantly downregulated in RML prion-infected mice, but showed little change in mice inoculated with 301V prions. Most work toward developing anti-prion therapies has been carried out in short incubation time systems using RML or closely related prion isolates, suggesting that therapies for one prion strain or one host genotype may not be effective in other situations. The same considerations will probably hold in humans with different phenotypic types of prion diseases emerging from different prion mutations and as such indicates the importance of the emerging personalized medicine—treating individuals as individuals and not as a member of large populations (Price *et al*, 2008).

Another use of the systems medicine approach is to aid in the identification of genes that affect the pathogenesis of prion disease. For example, several studies have mapped genetic modifiers of prion susceptibility and incubation time (Prusiner and Kingsbury, 1985; Stephenson *et al*, 2000; Lloyd *et al*, 2001; Manolakou *et al*, 2001; Moreno *et al*, 2003). Prion-specific DEGs that are located in chromosomal regions containing modifier genes are priority candidates for the genes underlying modulation of prion incubation time.

Genetically modified mice whose prion incubation times reflect levels of PrP expression help discriminate among genes relevant to prion replication, pathological changes, and clinical disease. It is striking that disease progression is slow in the heterozygous 0/+ mice, although PrP^{Sc} accumulates to levels comparable to those in diseased wild-type mice long before clinical signs occur. Most (311/333) DEGs shared among B6-RML, B6-301V, B6.I-RML, B6.I-301V, and FVB-RML also show similar patterns of change in 0/+ mice. The onset of differential expression occurs later in 0/+ mice than in the other combinations, presumably reflecting the reduced supply of PrP^{C} for conversion to PrP^{Sc}, but, in most cases, the elevated or reduced levels of DEGs persists for a much greater proportion of the incubation period. These results suggest that fundamental processes are shared among 0/+ mice and our core panel, and the long incubation time due to reduced PrP^{C} levels reflects the time required for accumulation of sufficient neurological damage. Degradation of pathogenically relevant PrP^{Sc} from the brain could also be more efficient in 0/+ mice (Safar *et al*, 2005) and thus account for some of this effect.

On the other hand, RML-infected Tg4053 mice, overexpressing PrP, showed significant changes in 125 of the 333 DEGs in the shared set. Prominent shared DEGs in most of the key shared modules exhibited similar patterns in Tg4053 mice, though generally of smaller in magnitude and closer in time to clinical illness and death than all other combinations (see Figure 3). This suggests that similar pathological responses and processes associated with prion replication are occurring in PrP-overexpressing mice in accord with the similar end-stage pathology typical for RML prion-infected mice. Although perturbed networks and modules in the other combinations were generally shared by Tg4053, there was also a unique set of highly significant DEGs in these transgenic mice (Figure 2C). The very short incubation time of Tg4053 reflects the increased supply of PrP^{C} for conversion to PrP^{Sc} and expression of the Tg4053-specific DEGs changed soon after infection. The Tg4053 set may reflect networks perturbed by prion replication. Alternatively, the overexpression of PrP may induce novel replication and disease pathways and affect cell types that are not prominent in the other mouse strain–prion

strain combinations. It is important to stress, for both Tg4053 and the other combinations, that changes in the levels of expression can reflect changes in transcription, changes in mRNA turnover, loss of specific cell types, or loss of specialized structures such as synapses that may harbor select mRNAs. It is likely that our results reflect all of these mechanisms. For example, the increased levels of glial DEGs in the brain can reflect both activation of the cells and cell proliferation or influx of microglial precursors as suggested by the perturbation in the leukocyte extravasation module (Figure 5). It is also worth noting that the inconsistent and large changes in expression that are seen in many genes after clinical disease appears are likely to reflect cell death and nonspecific changes due to illness.

Although there is clear correspondence between pathological events and changes in gene expression in relevant networks and modules, it is not clear which, if any, of the changes are specific to prion infection. Not surprisingly, many of the shared prion DEGs have been seen in other neurodegenerative diseases, where similar pathological events such as gliosis, synaptic degeneration, and neuron loss occur. Dynamic analysis of changes in gene expression during the course of neurodegenerative diseases in humans is difficult, but analyses similar to ours have been performed in transgenic mouse models. Several previous studies on mice overexpressing Alzheimer's amyloid precursor protein (APP) demonstrated involvement of similar networks. A limitation of these studies is the failure of Tg(APP) mice to recapitulate the neurofibrillary tangles and neuron loss of Alzheimer's patients. Particularly informative are the kinetic analyses by Y Wakutani and P St George-Hyslop (personal communication) on the perturbation of inflammatory pathways as amyloid accumulates in Tg(APP)CRND8 mice; these changes are similar to those seen in prion infection. Although no appreciable neuron loss occurs in TgCRND8 mice, synaptic loss and behavioral changes are observed. Overall, of 86 DEGs observed in TgCRND8 mice, 37 were observed as shared in our study (see Supplementary Tables S1 and S2) were seen as RML prion strain-enriched DEGs. Notable differences in DEG sets between prion-infected mice and TgCRND8 include the absence of PRR-related genes in TgCRND8 mice, whereas complement genes and glial markers are shared between the two disease models. Although similar processes, such as lipid metabolism, were perturbed in both systems, individual DEGs or the direction of changes for the same DEGs often differed. Most interesting examples are genes involved in cholesterol biosynthesis: these genes were decreased in RML prion-infected mice, whereas they were upregulated in TgCRND8 mice. Whether any of the DEGs that appear to be markers for prion infection actually are specific for prion disease will require further investigation. It is striking that even including our novel modules, nearly one-third of our shared DEGs could not be assigned to a hypothetical prion disease network. Such genes represent the 'dark genes' of prion disease and suggest that all diseases will be far more complex than initially thought. This is a compelling argument for using the global or comprehensive analyses of systems approaches.

Although associating DEGs to pathological events is relatively straightforward, identifying genes as specifically involved in or perturbed by the process of conversion of PrP^{C} to PrP^{Sc} is more difficult. Addition of brain homogenate greatly facilitates the conversion of purified PrP^{C} *in vitro* protein-mediated cyclic amplification reactions (Soto *et al*, 2005) and an unknown factor that binds to a C-terminal region of PrP may be limiting for cross-species transmission as a facilitator of conversion (Kaneko *et al*, 1997). Various prion infection-specific DEGs have been reported in N2a cells, which do not exhibit severe cellular abnormalities due to prion replication. However, systematic analysis of N2a sublines independently infected with scrapie prions did not reveal any set of shared DEGs indicative of prion infection that were common to all sublines (Chasseigneaux *et al*, 2008). Although this is likely due to the instability and aneuploidy of N2a cells, the possibility that gene expression is only moderately perturbed by the conversion process must be considered. The fact that mRNA levels for arguably the most important molecule in prion disease, PrP, do not change during the course of infection was confirmed in this study (difference of the *Prnp* mRNA levels between infected and normal brains were not significant). This lack of change originally led some to conclude that PrP was not central to disease (Chesebro *et al*, 1985). Other post-translational changes, such as elevation of the Notch intracellular domain that has been demonstrated to play a role in prion disease (Ishikura *et al*, 2005), would not be detected in our study. Similarly, levels of the PrP-related protein Shadoo have been reported to decrease in prion-diseased mice (Watts *et al*, 2007), but expression of its mRNA (*Sprn*) is unchanged; the relevance of changes in Shadoo levels to prion disease is as yet uncertain.

A systems approach to discover early, reliable diagnostic markers has drawn significant attention in prion disease because definitive diagnosis currently requires post-mortem immunological analysis of brain tissues (Safar *et al*, 1998; Soto, 2004; Glatzel *et al*, 2005). As an alternative, early and reliable blood assays would be very desirable, especially to prevent the spread of the disease through blood transfusion or consumption of prion-infected animal meat. Currently, advanced blood assay technologies still focus on the detection of very low levels of PrP^{Sc} in blood. Cyclic amplification of the PrP^{Sc} protein from blood of affected animals has been achieved (Saa *et al*, 2006), but sensitivity is as yet too low (only 60% of prion-infected animals tested positive) for routine application to preclinical diagnosis. In this regard, the shared DEGs uniquely associated with prion pathophysiology and secreted into the blood offer new opportunities for the identification of diagnostic marker candidates for robust blood assays, as some of the expression changes are expected to be reflected as changes in the levels of disease-perturbed brain proteins secreted into the peripheral blood. Preliminary observations suggest that this will be a powerful approach to early diagnosis of prion disease. H Yoo and L Hood (unpublished observations) used selected prion-specific DEGs as biomarker candidates in conjunction with mass spectrometry-based proteomics analyses to identify multiple secreted proteins as potential diagnostic serum biomarkers of prion disease. The important point is that a systems approach to disease will, through the formulation of testable hypotheses, lead to deeper mechanistic insights into the disease process and will as well lead to powerful new approaches to early (preclinical)

diagnosis and therapy (using drugs to re-engineer disease-perturbed networks to make them behave in a more normal manner—or at least abrogate the more deleterious aspects of their function). In a more conventional approach to therapy, this network analysis will reveal key nodal points that may themselves become targets for drugs. In either case, the systems approach to disease does open up powerful new approaches to the identification of targets for drug therapy.

It is clear that these network studies reflect the dynamics of the prion infectious process—at this time they have not provided insights into the initiating mechanism(s) of disease. We should stress that there are not a sufficient number of informative time points during the early stages of the prion disease to identify the initial changes induced by infection. Moreover, the dilution of signal from these earliest changes that would have occurred initially in a small number of cells might well be beyond the resolution of these studies conducted on whole brain, suggesting that early samples of thalamus, where prion replication is first detected, may be more informative. In spite of this, we have detected dynamically changing series of brain networks that have relevance to the changing pathophysiology of the disease. We plan to follow up these studies with the infection of CNS stem cell-containing brain neurospheres *in vitro* (Giri *et al*, 2006). In these cell lines, we should be able to detect very early events, at the expense of losing the context of the intact brain and its multiplicity of cellular interactions.

We have demonstrated here the power of comprehensive, global approaches to systems as complex as prion disease, even when the data sets are restricted to gene expression profiles, and involve whole brain. The efficacy of using several strain combinations, prion and genetic backgrounds as a biological filter to deal with signal-to-noise issues and identify the network signals that are important for various disease-related processes is a striking lesson from our study. The new modules that have been connected to the disease, the strong alignment of the specific pathogenic processes with network changes, and the range of novel and sharpened hypotheses illustrate the power of this approach. We have confidence that with the addition of other data types, the attribution of network processes to brain regions and cell types, and the specific testing of hypotheses suggested here, that the systems medicine of prion disease (and other neurodegenerative diseases) will advance rapidly.

Materials and methods

Mice and scrapie infection

B6, B6.I, FVB, 0/+, 0/0, and Tg4053 mice were used. Female mice (C57BL/6 and others) were inoculated intracerebrally at 5 weeks of age with 10 μl of 10% brain homogenate from clinically ill mice or normal control mice. Two prion strains were used: RML and 301V. Mice were killed at the intervals indicated in Table I for RNA preparation and brain histoblots. Clinical signs at the time of killing were noted.

RNA preparation and microarray analysis

Total RNA was extracted from each mouse brain using TRIZOL reagent (Invitrogen, USA), was treated with *DNase I* (Ambion), and further purified with RNeasy columns (Qiagen, USA). Quality of RNA samples was evaluated by using BioAnalyzer (Agilent, USA). Here, 5 μg of total RNA was reverse transcribed and followed by generation of double-stranded cDNAs. The resulting double-stranded cDNAs were purified and biotinylated to cRNAs. The labeled antisense cRNAs were fragmented and hybridized to GeneChip Mouse Genome 430 2.0 Array (Affymetrix, USA), which contains 45 000 probe sets. The hybridization was carried out for 16 h at 45°C. The arrays were washed and stained with streptavidin phycoerythrin using a GeneChip Fluidics Station 450 (Affymetrix) and scanned using a GeneChip scanner 3000 (Affymetrix). The scanned images of the arrays were converted and imported into the ISB's Systems Biology Experiment Analysis System (SBEAMS) for array data normalization and further analyses.

Identification of shared DEGs across the five prion–mouse combinations

To identify the genes involved in essential processes related to prion pathogenesis, we identified the DEGs with shared differential expression patterns in five prion–mouse combinations (B6-RML, B6.I-301V, B6-301V, B6.I-RML, and FVB-RML). The following method was applied: (i) log2 median ratios at each time point were computed in all five core combinations; (ii) the time points in each prion–mouse combination are normalized by its incubation time, and the log2 median ratios for each gene at the normalized time points are then scaled into those with zero mean and unit variance; (iii) these scaled median ratios from the five combinations were combined, and a smoothing line was then fit using super smoothing method (Friedman and Stuetzle, 1982) to the combined median ratios to compute a goodness of fit measure, a normalized ratio of sum of squared regression to sum of squared error (Supplementary information)—for a gene whose normalized temporal expression patterns are well-correlated, a high goodness of fit measure is produced; (iv) to perform an empirical statistical hypothesis testing, a control data set was generated using Monte Carlo simulation by randomly sampling the five combination data (Supplementary information); (v) goodness of fit measures were then computed for the genes in the randomly sampled data set—the computed goodness of fit measures are not large because they should not be systematically correlated in the random data; (vi) a null hypothesis distribution (pdf(H0)) was then empirically driven using Gaussian kernel density estimation for the computed goodness of fit measures; and (vii) a *P*-value of a gene being correlated by chance across the five combinations was then calculated using pdf(H0) by one-sided test of the corresponding goodness of fit measure computed in step (iii) (Supplementary information). A gene with a small *P*-value shows well-shared patterns across the five core combinations. In addition to the correlation in temporal expressions, the shared DEGs should also be differentially expressed in all combinations (Supplementary information). Thus, *P*-values of genes being differentially expressed in all five combinations were computed by combining the five *P*-values (Supplementary information). Finally, both *P*-values for correlation and combined *P*-values for differential expression are then combined using Stouffer's method (Hwang *et al*, 2005), resulting in the overall *P*-values of genes showing shared differential temporal patterns. A gene with a small overall *P*-value shows well-shared differential patterns. To stringently identify the shared DEGs, we selected shared DEGs using a cutoff for the overall *P*-values of 10^{-3}. Then, we further removed potential false positives as follows: for each selected shared DEG, (1) the maximum *P*-value (P_{max}) of those computed for differential expression in the five mouse–prion combinations (PB6-RML, PB6.I-301V, PB6-301V, PB6.I-RML, and PFVB-RML; Supplementary information) was computed; (2) the maximum absolute fold changes in the individual combinations (T_{max}(B6-RML), T_{max}(B6.I-301V), T_{max}(B6-301V), T_{max}(B6.I-RML), and T_{max}(FVB-RML)) were computed; and (3) the selected genes were considered and removed as false positives if at least one of the five P_{max} values was larger than 0.1 and at least one of the five T_{max} values from the five combinations was smaller than 1.5 at the same time.

Typical time course analyses mainly detect differential expression in the individual time course data (Supplementary information). Unlike these methods, our method focuses on detecting shared patterns among differential expression from multiple time course data sets differing in numbers of time points, sampling intervals, and time spans

at the expense of ignoring differential expression not common in all multiple time course data sets.

Identification of incubation time- and prion-specific genes

To identify the genes involved in biological processes that are activated only in mice with short incubation times and also a particular prion strain, the following method was applied: (i) a training set of the genes showing incubation time-specific (or RML-specific) differential expression was identified by examining false positives that were removed from the shared DEGs selected with a relaxed cutoff of $P<0.01$; (ii) after smoothing expression profiles of the genes in the training set using a moving average method (window size=5), the reference temporal profiles were defined for the genes in the training set as the median profile of smoothed log2 temporal ratios; (iii) for each gene, the correlation (also *t*-statistic value) of the smoothed log2 temporal profile with the reference profile was computed; (iv) as done in the previous empirical statistical hypothesis testing, the null hypothesis distribution was then estimated after generating a randomized control data set and computing the correlation and *t*-statistic values with the reference profile; and (v) using $pdf(H_0)$, a *P*-value was computed for each gene. Finally, a set of incubation time-specific (or RML-specific) genes was identified using a stringent cutoff ($P<10^{-4}$). We also further removed potential false positives when a *P*-value for differential expressions in short incubation time (or RML) combinations was at least larger than 0.1 and also a *P*-value in long incubation time (or FVB) combinations was at least less than 0.1, respectively. See further details in the Supplementary information.

Supplementary information

Supplementary information is available at the *Molecular Systems Biology* website (www.nature.com/msb).

Acknowledgements

We thank the MRI Animal Resource Facility staff for animal care. We thank Bruz Marzolf and Krassen Dimitrov at the microarray core facility at ISB for technical support. We also thank David Galas and Gilbert Omenn for thorough reviews. We thank Gustavo Glusman for his assistance in visualizing time series expression profiles with circular heatmaps. We are grateful to Alan Aderem, John Bermingham, Ranjit Giri, and Rajeev Kumar for helpful discussions. This study was supported by grants from the National Prion Research Program, US Department of Defense (Grants DAMD17-03-1-0321 and DAMD17-03-1-0425) and from NIH grants NS41997 and GM076547.

Conflict of interest

The authors declare that they have no conflict of interest.

References

Baranano DE, Rao M, Ferris CD, Snyder SH (2002) Biliverdin reductase: a major physiologic cytoprotectant. *Proc Natl Acad Sci USA* **99:** 16093–16098

Basu S, Mohan ML, Luo X, Kundu B, Kong Q, Singh N (2007) Modulation of proteinase K-resistant prion protein in cells and infectious brain homogenate by redox iron: implications for prion replication and disease pathogenesis. *Mol Biol Cell* **18:** 3302–3312

Baumann F, Tolnay M, Brabeck C, Pahnke J, Kloz U, Niemann HH, Heikenwalder M, Rulicke T, Burkle A, Aguzzi A (2007) Lethal recessive myelin toxicity of prion protein lacking its central domain. *EMBO J* **26:** 538–547

Ben-Zaken O, Tzaban S, Tal Y, Horonchik L, Esko JD, Vlodavsky I, Taraboulos A (2003) Cellular heparan sulfate participates in the metabolism of prions. *J Biol Chem* **278:** 40041–40049

Berriz GF, King OD, Bryant B, Sander C, Roth FP (2003) Characterizing gene sets with FuncAssociate. *Bioinformatics* **19:** 2502–2504

Block ML, Zecca L, Hong JS (2007) Microglia-mediated neurotoxicity: uncovering the molecular mechanisms. *Nat Rev Neurosci* **8:** 57–69

Booth S, Bowman C, Baumgartner R, Sorensen G, Robertson C, Coulthart M, Phillipson C, Somorjai RL (2004) Identification of central nervous system genes involved in the host response to the scrapie agent during preclinical and clinical infection. *J Gen Virol* **85:** 3459–3471

Bossy-Wetzel E, Schwarzenbacher R, Lipton SA (2004) Molecular pathways to neurodegeneration. *Nat Med* **10** (Suppl)**:** S2–S9

Bouzamondo-Bernstein E, Hopkins SD, Spilman P, Uyehara-Lock J, Deering C, Safar J, Prusiner SB, Ralston III HJ, DeArmond SJ (2004) The neurodegeneration sequence in prion diseases: evidence from functional, morphological and ultrastructural studies of the GABAergic system. *J Neuropathol Exp Neurol* **63:** 882–899

Bouzamondo E, Milroy AM, Ralston III HJ, Prusiner SB, DeArmond SJ (2000) Selective neuronal vulnerability during experimental scrapie infection: insights from an ultrastructural investigation. *Brain Res* **874:** 210–215

Brown AR, Rebus S, McKimmie CS, Robertson K, Williams A, Fazakerley JK (2005) Gene expression profiling of the preclinical scrapie-infected hippocampus. *Biochem Biophys Res Commun* **334:** 86–95

Brown DR (2001) Microglia and prion disease. *Microsc Res Tech* **54:** 71–80

Brown HC, Castano A, Fearn S, Townsend M, Edwards G, Streuli C, Perry VH (1997) Adhesion molecules involved in macrophage responses to Wallerian degeneration in the murine peripheral nervous system. *Eur J Neurosci* **9:** 2057–2063

Bruce ME, McBride PA, Jeffrey M, Scott JR (1994) PrP in pathology and pathogenesis in scrapie-infected mice. *Mol Neurobiol* **8:** 105–112

Bueler H, Aguzzi A, Sailer A, Greiner RA, Autenried P, Aguet M, Weissmann C (1993) Mice devoid of PrP are resistant to scrapie. *Cell* **73:** 1339–1347

Bueler H, Raeber A, Sailer A, Fischer M, Aguzzi A, Weissmann C (1994) High prion and PrPSc levels but delayed onset of disease in scrapie-inoculated mice heterozygous for a disrupted PrP gene. *Mol Med* **1:** 19–30

Carlson GA, Ebeling C, Torchia M, Westaway D, Prusiner SB (1993) Delimiting the location of the scrapie prion incubation time gene on chromosome 2 of the mouse. *Genetics* **133:** 979–988

Carlson GA, Ebeling C, Yang SL, Telling G, Torchia M, Groth D, Westaway D, DeArmond SJ, Prusiner SB (1994) Prion isolate specified allotypic interactions between the cellular and scrapie prion proteins in congenic and transgenic mice. *Proc Natl Acad Sci USA* **91:** 5690–5694

Chasseigneaux S, Pastore M, Britton-Davidian J, Manie E, Stern MH, Callebert J, Catalan J, Casanova D, Belondrade M, Provansal M, Zhang Y, Burkle A, Laplanche JL, Sevenet N, Lehmann S (2008) Genetic heterogeneity versus molecular analysis of prion susceptibility in neuroblasma N2a sublines. *Arch Virol* **153:** 1693–1702

Chesebro B, Race R, Wehrly K, Nishio J, Bloom M, Lechner D, Bergstrom S, Robbins K, Mayer L, Keith JM, Garon C, Haase A (1985) Identification of scrapie prion protein-specific mRNA in scrapie-infected and uninfected brain. *Nature* **315:** 331–333

Connor JR, Menzies SL (1996) Relationship of iron to oligodendrocytes and myelination. *Glia* **17:** 83–93

Dandoy-Dron F, Guillo F, Benboudjema L, Deslys JP, Lasmezas C, Dormont D, Tovey MG, Dron M (1998) Gene expression in scrapie. Cloning of a new scrapie-responsive gene and the identification of increased levels of seven other mRNA transcripts. *J Biol Chem* **273:** 7691–7697

Deininger MH, Bekure-Nemariam K, Trautmann K, Morgalla M, Meyermann R, Schluesener HJ (2003) Cyclooxygenase-1 and -2 in brains of patients who died with sporadic Creutzfeldt–Jakob disease. *J Mol Neurosci* **20:** 25–30

Engelstein R, Ovadia H, Gabizon R (2007) Copaxone interferes with the PrP Sc–GAG interaction. *Eur J Neurol* **14:** 877–884

Friedman JH, Stuetzle W (1982) Projection pursuit methods for data analysis. In *Modern Data Analysis*. New York: Academic Press

Gabizon R, Meiner Z, Halimi M, Ben-Sasson SA (1993) Heparin-like molecules bind differentially to prion-proteins and change their intracellular metabolic fate. *J Cell Physiol* **157:** 319–325

Giese A, Brown DR, Groschup MH, Feldmann C, Haist I, Kretzschmar HA (1998) Role of microglia in neuronal cell death in prion disease. *Brain Pathol* **8:** 449–457

Giri RK, Young R, Pitstick R, DeArmond SJ, Prusiner SB, Carlson GA (2006) Prion infection of mouse neurospheres. *Proc Natl Acad Sci USA* **103:** 3875–3880

Glatzel M, Stoeck K, Seeger H, Luhrs T, Aguzzi A (2005) Human prion diseases: molecular and clinical aspects. *Arch Neurol* **62:** 545–552

Guentchev M, Groschup MH, Kordek R, Liberski PP, Budka H (1998) Severe, early and selective loss of a subpopulation of GABAergic inhibitory neurons in experimental transmissible spongiform encephalopathies. *Brain Pathol* **8:** 615–623

Guentchev M, Hainfellner JA, Trabattoni GR, Budka H (1997) Distribution of parvalbumin-immunoreactive neurons in brain correlates with hippocampal and temporal cortical pathology in Creutzfeldt–Jakob disease. *J Neuropathol Exp Neurol* **56:** 1119–1124

Guentchev M, Wanschitz J, Voigtlander T, Flicker H, Budka H (1999) Selective neuronal vulnerability in human prion diseases. Fatal familial insomnia differs from other types of prion diseases. *Am J Pathol* **155:** 1453–1457

Hijazi N, Kariv-Inbal Z, Gasset M, Gabizon R (2005) PrPSc incorporation to cells requires endogenous glycosaminoglycan expression. *J Biol Chem* **280:** 17057–17061

Hood L, Heath JR, Phelps ME, Lin B (2004) Systems biology and new technologies enable predictive and preventative medicine. *Science* **306:** 640–643

Horonchik L, Tzaban S, Ben-Zaken O, Yedidia Y, Rouvinski A, Papy-Garcia D, Barritault D, Vlodavsky I, Taraboulos A (2005) Heparan sulfate is a cellular receptor for purified infectious prions. *J Biol Chem* **280:** 17062–17067

Hwang D, Rust AG, Ramsey S, Smith JJ, Leslie DM, Weston AD, de Atauri P, Aitchison JD, Hood L, Siegel AF, Bolouri H (2005) A data integration methodology for systems biology. *Proc Natl Acad Sci USA* **102:** 17296–17301

Imamura Y, Katahira T, Kitamura D (2004) Identification and characterization of a novel BASH N terminus-associated protein, BNAS2. *J Biol Chem* **279:** 26425–26432

Ishikura N, Clever JL, Bouzamondo-Bernstein E, Samayoa E, Prusiner SB, Huang EJ, DeArmond SJ (2005) Notch-1 activation and dendritic atrophy in prion disease. *Proc Natl Acad Sci USA* **102:** 886–891

Jeffrey M, Halliday WG, Bell J, Johnston AR, MacLeod NK, Ingham C, Sayers AR, Brown DA, Fraser JR (2000) Synapse loss associated with abnormal PrP precedes neuronal degeneration in the scrapie-infected murine hippocampus. *Neuropathol Appl Neurobiol* **26:** 41–54

Jensen MB, Gonzalez B, Castellano B, Zimmer J (1994) Microglial and astroglial reactions to anterograde axonal degeneration: a histochemical and immunocytochemical study of the adult rat fascia dentata after entorhinal perforant path lesions. *Exp Brain Res* **98:** 245–260

Kaneko K, Zulianello L, Scott M, Cooper CM, Wallace AC, James TL, Cohen FE, Prusiner SB (1997) Evidence for protein X binding to a discontinuous epitope on the cellular prion protein during scrapie prion propagation. *Proc Natl Acad Sci USA* **94:** 10069–10074

Kikuta Y, Kasyu H, Kusunose E, Kusunose M (2000) Expression and catalytic activity of mouse leukotriene B4 omega-hydroxylase, CYP4F14. *Arch Biochem Biophys* **383:** 225–232

Kim NH, Park SJ, Jin JK, Kwon MS, Choi EK, Carp RI, Kim YS (2000) Increased ferric iron content and iron-induced oxidative stress in the brains of scrapie-infected mice. *Brain Res* **884:** 98–103

Klein MA, Kaeser PS, Schwarz P, Weyd H, Xenarios I, Zinkernagel RM, Carroll MC, Verbeek JS, Botto M, Walport MJ, Molina H, Kalinke U, Acha-Orbea H, Aguzzi A (2001) Complement facilitates early prion pathogenesis. *Nat Med* **7:** 488–492

Klein TR, Kirsch D, Kaufmann R, Riesner D (1998) Prion rods contain small amounts of two host sphingolipids as revealed by thin-layer chromatography and mass spectrometry. *Biol Chem* **379:** 655–666

Klingenstein R, Lober S, Kujala P, Godsave S, Leliveld SR, Gmeiner P, Peters PJ, Korth C (2006) Tricyclic antidepressants, quinacrine and a novel, synthetic chimera thereof clear prions by destabilizing detergent-resistant membrane compartments. *J Neurochem* **98:** 748–759

Kristensson K, Feuerstein B, Taraboulos A, Hyun WC, Prusiner SB, DeArmond SJ (1993) Scrapie prions alter receptor-mediated calcium responses in cultured cells. *Neurology* **43:** 2335–2341

Lein ES, Hawrylycz MJ, Ao N, Ayres M, Bensinger A, Bernard A, Boe AF, Boguski MS, Brockway KS, Byrnes EJ, Chen L, Chen L, Chen TM, Chin MC, Chong J, Crook BE, Czaplinska A, Dang CN, Datta S, Dee NR *et al* (2007) Genome-wide atlas of gene expression in the adult mouse brain. *Nature* **445:** 168–176

Liberski PP, Sikorska B, Bratosiewicz-Wasik J, Gajdusek DC, Brown P (2004) Neuronal cell death in transmissible spongiform encephalopathies (prion diseases) revisited: from apoptosis to autophagy. *Int J Biochem Cell Biol* **36:** 2473–2490

Lloyd SE, Onwuazor ON, Beck JA, Mallinson G, Farrall M, Targonski P, Collinge J, Fisher EM (2001) Identification of multiple quantitative trait loci linked to prion disease incubation period in mice. *Proc Natl Acad Sci USA* **98:** 6279–6283

Manolakou K, Beaton J, McConnell I, Farquar C, Manson J, Hastie ND, Bruce M, Jackson IJ (2001) Genetic and environmental factors modify bovine spongiform encephalopathy incubation period in mice. *Proc Natl Acad Sci USA* **98:** 7402–7407

Manson JC, Clarke AR, McBride PA, McConnell I, Hope J (1994) PrP gene dosage determines the timing but not the final intensity or distribution of lesions in scrapie pathology. *Neurodegeneration* **3:** 331–340

Mayer-Sonnenfeld T, Avrahami D, Friedman-Levi Y, Gabizon R (2008) Chemically induced accumulation of GAGs delays PrP(Sc) clearance but prolongs prion disease incubation time. *Cell Mol Neurobiol* **28:** 1005–1015

Mayer-Sonnenfeld T, Zeigler M, Halimi M, Dayan Y, Herzog C, Lasmezas CI, Gabizon R (2005) The metabolism of glycosaminoglycans is impaired in prion diseases. *Neurobiol Dis* **20:** 738–743

Moreno CR, Lantier F, Lantier I, Sarradin P, Elsen JM (2003) Detection of new quantitative trait loci for susceptibility to transmissible spongiform encephalopathies in mice. *Genetics* **165:** 2085–2091

Moscarello MA, Mastronardi FG, Wood DD (2007) The role of citrullinated proteins suggests a novel mechanism in the pathogenesis of multiple sclerosis. *Neurochem Res* **32:** 251–256

Na YJ, Jin JK, Kim JI, Choi EK, Carp RI, Kim YS (2007) JAK–STAT signaling pathway mediates astrogliosis in brains of scrapie-infected mice. *J Neurochem* **103:** 637–649

Nakamura Y (2002) Regulating factors for microglial activation. *Biol Pharm Bull* **25:** 945–953

Ohno M, Aotani H, Shimada M (1995) Glial responses to hypoxic/ischemic encephalopathy in neonatal rat cerebrum. *Brain Res Dev Brain Res* **84:** 294–298

Ohya W, Funakoshi H, Kurosawa T, Nakamura T (2007) Hepatocyte growth factor (HGF) promotes oligodendrocyte progenitor cell proliferation and inhibits its differentiation during postnatal development in the rat. *Brain Res* **1147:** 51–65

Ortiz E, Pasquini JM, Thompson K, Felt B, Butkus G, Beard J, Connor JR (2004) Effect of manipulation of iron storage, transport, or availability on myelin composition and brain iron content in three different animal models. *J Neurosci Res* **77:** 681–689

Panickar KS, Norenberg MD (2005) Astrocytes in cerebral ischemic injury: morphological and general considerations. *Glia* **50:** 287–298

Papadopoulos V, Baraldi M, Guilarte TR, Knudsen TB, Lacapere JJ, Lindemann P, Norenberg MD, Nutt D, Weizman A, Zhang MR, Gavish M (2006) Translocator protein (18 kDa): new nomenclature for the peripheral-type benzodiazepine receptor based on its structure and molecular function. *Trends Pharmacol Sci* **27:** 402–409

Papadopoulos V, Brown AS (1995) Role of the peripheral-type benzodiazepine receptor and the polypeptide diazepam binding inhibitor in steroidogenesis. *J Steroid Biochem Mol Biol* **53:** 103–110

Perry VH, Cunningham C, Boche D (2002) Atypical inflammation in the central nervous system in prion disease. *Curr Opin Neurol* **15:** 349–354

Pikas DS, Li JP, Vlodavsky I, Lindahl U (1998) Substrate specificity of heparanases from human hepatoma and platelets. *J Biol Chem* **273:** 18770–18777

Plant SR, Wang Y, Vasseur S, Thrash JC, McMahon EJ, Bergstralh DT, Arnett HA, Miller SD, Carson MJ, Iovanna JL, Ting JP (2006) Upregulation of the stress-associated gene p8 in mouse models of demyelination and in multiple sclerosis tissues. *Glia* **53:** 529–537

Price ND, Edelman LB, Lee IY, Yoo H, Hwang D, Carlson GA, Galas DJ, Heath JR, Hood L (2008) Systems biology and systems medicine. In *Genomic and Personalized Medicine: from Principles to Practice*, Ginsburg G, Willard H (eds), Vol. 1, pp 74–85. New York: Elsevier

Priller J, Prinz M, Heikenwalder M, Zeller N, Schwarz P, Heppner FL, Aguzzi A (2006) Early and rapid engraftment of bone marrow-derived microglia in scrapie. *J Neurosci* **26:** 11753–11762

Prusiner SB (2003) An introduction to prion biology and disease. In *Prion Biology and Diseases*, 2nd edn, pp 1–88. Cold Spring Harbor: Cold Spring Harbor Laboratory Press

Prusiner SB, Kingsbury DT (1985) Prions—infectious pathogens causing the spongiform encephalopathies. *CRC Crit Rev Clin Neurobiol* **1:** 181–200

Rakonjac M, Fischer L, Provost P, Werz O, Steinhilber D, Samuelsson B, Radmark O (2006) Coactosin-like protein supports 5-lipoxygenase enzyme activity and up-regulates leukotriene A4 production. *Proc Natl Acad Sci USA* **103:** 13150–13155

Rezaie P, Lantos PL (2001) Microglia and the pathogenesis of spongiform encephalopathies. *Brain Res Brain Res Rev* **35:** 55–72

Riemer C, Neidhold S, Burwinkel M, Schwarz A, Schultz J, Kratzschmar J, Monning U, Baier M (2004) Gene expression profiling of scrapie-infected brain tissue. *Biochem Biophys Res Commun* **323:** 556–564

Rodriguez-Agudo D, Ren S, Wong E, Marques D, Redford K, Gil G, Hylemon P, Pandak WM (2008) Intracellular cholesterol transporter StarD4 binds free cholesterol and increases cholesteryl ester formation. *J Lipid Res* **49:** 1409–1419

Saa P, Castilla J, Soto C (2006) Presymptomatic detection of prions in blood. *Science* **313:** 92–94

Safar J, Wille H, Itri V, Groth D, Serban H, Torchia M, Cohen FE, Prusiner SB (1998) Eight prion strains have PrP(Sc) molecules with different conformations. *Nat Med* **4:** 1157–1165

Safar JG, DeArmond SJ, Kociuba K, Deering C, Didorenko S, Bouzamondo-Bernstein E, Prusiner SB, Tremblay P (2005) Prion clearance in bigenic mice. *J Gen Virol* **86:** 2913–2923

Sim RB, Kishore U, Villiers CL, Marche PN, Mitchell DA (2007) C1q binding and complement activation by prions and amyloids. *Immunology* **212:** 355–362

Simons K, Ehehalt R (2002) Cholesterol, lipid rafts, and disease. *J Clin Invest* **110:** 597–603

Skinner PJ, Abbassi H, Chesebro B, Race RE, Reilly C, Haase AT (2006) Gene expression alterations in brains of mice infected with three strains of scrapie. *BMC Genomics* **7:** 114

Sorensen G, Medina S, Parchaliuk D, Phillipson C, Robertson C, Booth SA (2008) Comprehensive transcriptional profiling of prion infection in mouse models reveals networks of responsive genes. *BMC Genomics* **9:** 114

Soto C (2004) Diagnosing prion diseases: needs, challenges and hopes. *Nat Rev Microbiol* **2:** 809–819

Soto C, Anderes L, Suardi S, Cardone F, Castilla J, Frossard MJ, Peano S, Saa P, Limido L, Carbonatto M, Ironside J, Torres JM, Pocchiari M, Tagliavini F (2005) Pre-symptomatic detection of prions by cyclic amplification of protein misfolding. *FEBS Lett* **579:** 638–642

Spires TL, Hannan AJ (2007) Molecular mechanisms mediating pathological plasticity in Huntington's disease and Alzheimer's disease. *J Neurochem* **100:** 874–882

Stephenson DA, Chiotti K, Ebeling C, Groth D, DeArmond SJ, Prusiner SB, Carlson GA (2000) Quantitative trait loci affecting prion incubation time in mice. *Genomics* **69:** 47–53

Vey M, Pilkuhn S, Wille H, Nixon R, DeArmond SJ, Smart EJ, Anderson RG, Taraboulos A, Prusiner SB (1996) Subcellular colocalization of the cellular and scrapie prion proteins in caveolae-like membranous domains. *Proc Natl Acad Sci USA* **93:** 14945–14949

Walis A, Liberski PP, Brown P (2004) Ultrastructural alterations in the optic nerve in transmissible spongiform encephalopathies or prion diseases––a review. *Folia Neuropathol* **42** (Suppl B)**:** 153–160

Wang M, Kong Q, Gonzalez FA, Sun G, Erb L, Seye C, Weisman GA (2005) P2Y nucleotide receptor interaction with alpha integrin mediates astrocyte migration. *J Neurochem* **95:** 630–640

Wang Y, Li T, Qiu X, Mo X, Zhang Y, Song Q, Ma D, Han W (2008) CMTM3 can affect the transcription activity of androgen receptor and inhibit the expression level of PSA in LNCaP cells. *Biochem Biophys Res Commun* **371:** 54–58

Watts JC, Drisaldi B, Ng V, Yang J, Strome B, Horne P, Sy MS, Yoong L, Young R, Mastrangelo P, Bergeron C, Fraser PE, Carlson GA, Mount HT, Schmitt-Ulms G, Westaway D (2007) The CNS glycoprotein Shadoo has PrP(C)-like protective properties and displays reduced levels in prion infections. *EMBO J* **26:** 4038–4050

Westaway D, Goodman PA, Mirenda CA, McKinley MP, Carlson GA, Prusiner SB (1987) Distinct prion proteins in short and long scrapie incubation period mice. *Cell* **51:** 651–662

Williams A, Lucassen PJ, Ritchie D, Bruce M (1997) PrP deposition, microglial activation, and neuronal apoptosis in murine scrapie. *Exp Neurol* **144:** 433–438

Wojtera M, Sikorska B, Sobow T, Liberski PP (2005) Microglial cells in neurodegenerative disorders. *Folia Neuropathol* **43:** 311–321

Wong K, Qiu Y, Hyun W, Nixon R, VanCleff J, Sanchez-Salazar J, Prusiner SB, DeArmond SJ (1996) Decreased receptor-mediated calcium response in prion-infected cells correlates with decreased membrane fluidity and IP3 release. *Neurology* **47:** 741–750

Xiang W, Hummel M, Mitteregger G, Pace C, Windl O, Mansmann U, Kretzschmar HA (2007) Transcriptome analysis reveals altered cholesterol metabolism during the neurodegeneration in mouse scrapie model. *J Neurochem* **102:** 834–847

Xiang W, Windl O, Wunsch G, Dugas M, Kohlmann A, Dierkes N, Westner IM, Kretzschmar HA (2004) Identification of differentially expressed genes in scrapie-infected mouse brains by using global gene expression technology. *J Virol* **78:** 11051–11060

Zhang Y, Spiess E, Groschup MH, Burkle A (2003) Up-regulation of cathepsin B and cathepsin L activities in scrapie-infected mouse Neuro2a cells. *J Gen Virol* **84:** 2279–2283